Title (50-word maximum): Repeated administration of 2-hydroxypropyl-β-cyclodextrin (HPβCD) attenuates the chronic inflammatory response to experimental stroke

Abbreviated Title (50-character maximum): HPβCD attenuates chronic inflammation after stroke

Danielle A. Becktel[1], Jacob C. Zbesko[1], Jennifer B. Frye[1], Amanda G. Chung[1], Megan Hayes[1], Kylie Calderon[1], Jeffrey W. Grover[2], Anna Li[1,3], Frankie G. Garcia[1], Marco A. Tavera-Garcia[1], Rick G. Schnellmann[4], Hsin-Jung Joyce Wu[1,3], Thuy-Vi V. Nguyen[1,5], Kristian P. Doyle*[1,5,6,7,8,9]

[1]Department of Immunobiology, University of Arizona, Tucson, Arizona, 85719, USA
[2]Department of Molecular and Cellular Biology, University of Arizona, Tucson, Arizona, 85719, USA
[3]Arizona Arthritis Center, University of Arizona, Tucson, Arizona, 85719
[4]Department of Pharmacology and Toxicology, University of Arizona, Tucson, Arizona, 85719, USA
[5]Department of Neurology, University of Arizona, Tucson, Arizona, 85719, USA
[6]BIO5 Institute, University of Arizona, Tucson, Arizona, 85719, USA
[7]Arizona Center on Aging, University of Arizona, Tucson, Arizona, 85719, USA
[8]Department of Psychology, University of Arizona, Tucson, Arizona, 85719, USA
[9]Department of Neurosurgery, University of Arizona, Tucson, Arizona, 85719, USA

*To whom correspondence should be addressed

Address for Correspondence:

Kristian P. Doyle, Ph.D.

Department of Immunobiology

University of Arizona

1656 E. Mabel Street, P.O. Box 245221

Tucson, Arizona, 85719

Tel: (1) 520-626-7013

Email: doylekr@arizona.edu

# of Figures: 14

# of Tables: 1 (No multimedia or 3D models in this manuscript)

# of Words in Abstract: 244

# of Words in Introduction: 586

# of Words in Discussion: 1296

Conflict of Interest Statement: The authors declare no competing financial interests.

Acknowledgments: This work was funded by NINDS R01NS096091 (KPD), NIA R01AG063808 (TVN), NIA R21AG062781 (TVN), United States Department of Veterans Affairs I01RX003224 (RGS), NIA T32AG058503-01A1 (DAB), NINDS F31NS105455 (JCZ), and the Fondation Leducq Transatlantic Network of Excellence

Stroke-IMPaCT (KPD). We thank Dr. Oswald Quehenberger (UCSD Lipidomics Core), Branden Lau, and Jonathan Galina-Mehlman (University of Arizona Genetics Core) for their technical assistance with lipidomics and transcriptomics analyses. We also thank Dr. Julia Slone-Murphy (NeuroEdit Ltd) for editing a draft of this manuscript.

Abstract (250 words maximum, including citations)

Globally, more than 67 million people are living with the effects of ischemic stroke. Importantly, many stroke survivors develop a chronic inflammatory response that contributes to cognitive impairment, a common and debilitating sequela of stroke that is insufficiently studied and currently untreatable. 2-hydroxypropyl-β-cyclodextrin (HPβCD) is an FDA-approved cyclic oligosaccharide developed to solubilize and entrap lipophilic substances. The goal of the present study was to determine whether the repeated administration of HPβCD curtails the chronic inflammatory response to stroke by reducing lipid accumulation within stroke infarcts in a distal middle cerebral artery occlusion + hypoxia (DH) mouse model of stroke. We subcutaneously injected young adult and aged mice with vehicle or HPβCD three times per week for up to 7 weeks following stroke and evaluated them using immunostaining, RNA sequencing, lipidomics, and behavioral analyses. Chronic stroke infarct and peri-infarct regions of HPβCD-treated mice were characterized by an upregulation of genes involved in lipid metabolism and a downregulation of genes involved in innate and adaptive immunity, reactive astrogliosis, and chemotaxis. Correspondingly, HPβCD reduced the accumulation of lipid droplets, T lymphocytes, B lymphocytes, and plasma cells in

stroke infarcts. Repeated administration of HPβCD also improved recovery through the preservation of neurons in the striatum and thalamus, induction of c-Fos in hippocampal regions, protection of hippocampal-dependent spatial working memory, and reduction in impulsivity at 7 weeks after stroke. These results indicate that systemic HPβCD treatment following stroke attenuates chronic inflammation and secondary neurodegeneration and prevents post-stroke cognitive decline.

Significance Statement (120 words maximum)

Dementia is a common and debilitating sequela of stroke. Currently, there are no available treatments for post-stroke dementia. Our study shows that lipid metabolism is disrupted in chronic stroke infarcts, which causes an accumulation of uncleared lipid debris and correlates with a chronic inflammatory response. To our knowledge, these substantial changes in lipid homeostasis have not been previously recognized or investigated in the context of ischemic stroke. We also provide a proof of principle that solubilizing and entrapping lipophilic substances using HPβCD could be an effective strategy for treating chronic inflammation after stroke and other CNS injuries. We propose that using HPβCD for the prevention of post-stroke dementia could improve recovery and increase long-term quality of life in stroke sufferers.

Introduction (650 words maximum, including citations)

Ischemic stroke is a leading cause of death and disability worldwide (Virani et al., 2020). Of stroke survivors, approximately one-third develop a delayed and progressive form of cognitive decline (Black, 2011); however, there are currently no targeted pharmacological interventions to prevent chronic neurodegeneration after stroke. With an aging global population, there is an increasing need for novel and effective treatments intended to resolve the chronic inflammatory response and promote functional recovery after stroke.

We previously reported, in a mouse model of post-stroke dementia, that delayed cognitive impairment is caused by a chronic inflammatory response to stroke that is mediated in part by B lymphocytes (Doyle et al., 2015; Doyle, Fathali, Siddiqui, & Buckwalter, 2012). In addition to the progressive infiltration of B lymphocytes, T lymphocytes, and IgA+ plasma cells into the infarct in the weeks following stroke, the chronic inflammatory response is also characterized by the production of neurotoxic molecules such as antibodies, cytokines, and degradative enzymes (Zbesko et al., 2020; Zbesko et al., 2018). These neurotoxic molecules permeate the glial scar and promote chronic inflammation and secondary neurodegeneration in the surrounding parenchyma (Zbesko et al., 2018). Notably, the chronic inflammatory response to stroke has a similar cellular and molecular profile to atherosclerosis. Chronic stroke infarcts contain foamy macrophages, lipid droplets, and intracellular and extracellular cholesterol crystals (Chung et al., 2018). These distinguishing characteristics are caused by overwhelmed lipid processing systems within macrophages, resulting in the

114 recruitment of adaptive immune cells and the production of pro-inflammatory cytokines
115 and degradative enzymes.
116
117 Lipids are principal structural components of the myelin sheath and are major
118 constituents of the human brain (Vance, 2012). Therefore, it is likely that foamy
119 macrophages and cholesterol crystals form in infarcts following ischemic stroke
120 because lipid debris derived from the breakdown of myelin and other cell membranes
121 overwhelms the processing capacity of infiltrating macrophages and resident microglia
122 (Cantuti-Castelvetri et al., 2018). 2-hydroxypropyl-β-cyclodextrin (HPβCD) is a U.S.
123 Food and Drug Administration-approved compound that entraps lipids and promotes
124 liver X receptor-mediated transcriptional reprogramming in macrophages to improve
125 cholesterol efflux and incite anti-inflammatory mechanisms (Zimmer et al., 2016).
126 Importantly, HPβCD reduces lipid levels in the lesion following spinal cord injury (Mar et
127 al., 2016) and prevents lipid overload within phagocytic cells in atherosclerosis and
128 Niemann–Pick disease type C (Taylor et al., 2012; Matsuo et al., 2013; Zimmer et al.,
129 2016). Thus, administration of HPβCD represents a multi-pronged approach to
130 mitigating lipid accumulation in phagocytic cells following ischemic stroke.
131
132 The overarching goal of this study was to investigate the efficacy of HPβCD as a
133 potential treatment for chronic inflammation and delayed cognitive impairment following
134 ischemic stroke. The aims of the current study were 2-fold: (1) to characterize the
135 lipidome of chronic stroke infarcts and (2) to determine whether lipid complexation and
136 macrophage reprogramming within infarcts, via the repeated systemic administration of

HPβCD, attenuates chronic inflammation and secondary neurodegeneration following stroke. To accomplish these aims, we used the distal middle cerebral artery occlusion + hypoxia mouse model of ischemic stroke in conjunction with immunohistochemistry, RNA-Seq, lipidomics, and behavioral analyses. Our resulting data indicate that, coincident with the substantial accumulation of infiltrating immune cells (Doyle et al., 2015; Zbesko et al., 2020), chronic stroke infarcts amass lipids, including sphingomyelins, cholesterol esters, and sulfatides. We also demonstrate that repeated administration of HPβCD in young adult and aged mice attenuates immune cell and lipid accumulation within chronic stroke infarcts and improves recovery at transcriptional and functional levels. Therefore, HPβCD has the potential to improve stroke recovery and prevent post-stroke dementia in humans.

Materials and Methods

Experimental design and statistical analysis

Experiments were designed using power analyses to determine sample sizes based on expected variances and group differences. Statistical analyses were performed with Prism 6.0 (GraphPad). Data are presented as the mean ± standard error of mean (SEM). Group sizes, statistical tests, and *p* values for each experiment are reported in **Table 1**. For GSEA, the normalized enrichment score (NES) is reported. The NES accounts for differences in gene set size and in correlations between gene sets. The NES is based on all dataset permutations to correct for multiple hypothesis testing.

Mice

Young adult (3- to 4-month-old) and aged (17- to 18-month-old) wild-type male C57BL/6J mice (Jackson Laboratory, Stock No. 000664) were used. Mice were housed in a temperature-controlled suite under a 12-hour light–dark regimen, with food and water available *ad libitum*. All procedures met NIH guidelines and were approved by the University of Arizona Institutional Animal Care and Use Committee. At each time point, mice were euthanized by isoflurane anesthesia (JD Medical), exsanguination, and subsequent intracardial perfusion with 0.9% saline. Whole brains or individual brain regions were then removed and either placed in RNAlater (Invitrogen, Cat. No. AM7020) for RNA sequencing analysis; flash frozen in liquid nitrogen for lipidomics analysis; or placed in a 4% paraformaldehyde (PFA) solution for 24 h before being transferred into a 30% sucrose solution for immunostaining analysis. Whole blood collected at the time of euthanasia was either placed directly in heparin-coated tubes for complete blood count analysis or extracted with sodium citrate to separate plasma via centrifugation.

Stroke surgeries

Stroke was induced in mice using the distal middle cerebral artery occlusion + hypoxia (DH) model. The DH stroke model generates a sizable infarct (24% of the ipsilateral hemisphere centered on the somatosensory cortex), has little variability, and has exceptional long-term survivability (Doyle et al., 2012; Nguyen et al., 2016). To induce stroke, we anesthetized animals by isoflurane inhalation and kept them at 37°C throughout the surgical procedure. For all experiments, we injected mice

subcutaneously (s.c.) with a single dose of buprenorphine hydrochloride (0.1 mg/kg; Henry Schein) and a single dose of cefazolin antibiotic (25 mg/kg; Sigma-Aldrich) dissolved in sterile saline. Following pre-operative preparation, the skull was exposed by creating a surgical incision in the skin and temporalis muscle. The right middle cerebral artery was visually identified, and a microdrill was used to expose it. The meninges were cut, and the vessel was cauterized using a small vessel cauterizer (Bovie Medical Corporation). Surgical wounds were closed using Surgi-lock 2oc tissue adhesive (Meridian Animal Health). We then immediately transferred mice to a hypoxia chamber (Coy Laboratory Products) containing 9% oxygen and 91% nitrogen for 45 min. Sustained-release buprenorphine (Bup-SR, 1 mg/kg s.c.; ZooPharm) was administered 24 h after surgery as post-operative analgesia.

Drug treatment

We injected HPβCD or vehicle s.c. three times per week, beginning 7 days after stroke surgery, for 6 weeks until euthanasia at 7 weeks after stroke. Mice in the treatment group received 2-hydroxypropyl-β-cyclodextrin powder (Sigma-Aldrich, Cat. No. H-107) dissolved in sterile phosphate-buffered saline (PBS) at a dose of 4 g HPβCD/kg body weight. Mice in the vehicle control group received 300 µL sterile PBS.

Immunostaining

Coronal brain sections (40 µm) were collected using a freezing Microm HM 450 sliding microtome (Thermo Fisher Scientific) and stored in cryoprotectant medium at –20°C until processing. Immunostaining was performed on free-floating brain sections using

206 standard protocols (Doyle et al., 2015; Nguyen et al., 2016; Zbesko et al., 2018).
207 Primary antibodies against neuronal nuclei (NeuN; 1:500; Millipore Sigma, Cat. No.
208 MAB377; RRID:AB_2298772), c-Fos (1:2000; Abcam, Cat. No. ab190289;
209 RRID:AB_2737414), CD3ε (1:1000; BD Biosciences, Cat. No. 550277;
210 RRID:AB_393573), B220/CD45R (1:500; BD Biosciences, Cat. No. 553085;
211 RRID:AB_394615), immunoglobulin A (IgA; 1:1000; BioLegend, Cat. No. 407004;
212 RRID:AB_315079), and CD138 (Syndecan-1; 1:200; BioLegend, Cat. No. 142514;
213 RRID:AB_2562198) were used in conjunction with the appropriate secondary antibody
214 and visualized using the VECTASTAIN Elite ABC Reagent, Peroxidase, R.T.U. (Vector
215 Laboratories, Cat. No. PK-7100) and Vector DAB Substrate (3,3'-diaminobenzidine) Kit
216 (Vector Laboratories, Cat. No. SK-4100). Secondary antibodies were diluted 1:400 for
217 biotinylated horse anti-mouse IgG (Vector Laboratories, Cat. No. BA-2000;
218 RRID:AB_2313581), biotinylated goat anti-hamster IgG (Vector Laboratories, Cat. No.
219 BA-9100; RRID:AB_2336137), and biotinylated rabbit anti-rat IgG (Vector Laboratories,
220 Cat. No. BA-4000; RRID:AB_2336206). Sections were imaged using a Keyence BZ-
221 X700 digital microscope with phase contrast, light, and fluorescence capabilities.
222
223 ***Oil Red O staining***
224 Frozen tissue sections were mounted on slides and allowed to dry. Mounted sections
225 were dehydrated in 100% propylene glycol for 5 min and then stained with Oil Red O
226 (ORO) for 10 min (Abcam, Cat. No. ab150678). The sections were then differentiated in
227 85% propylene glycol for 3 min and rinsed with distilled water three times. Coverslips
228 were applied to all slides using an aqueous mounting medium (Vector Laboratories,

Cat. No. H-1400). Stained sections were imaged with a Keyence BZ-X700 digital microscope.

Alcian blue staining

Frozen tissue sections were mounted on slides and allowed to dry. Slides were immersed in eosin (VWR, Cat. No. 95057-848) and then rinsed eight times in PBS. Slides were incubated in 3% acetic acid (pH 2.5) for 3 min and then placed in a solution of 1% w/v Alcian Blue in 3% acetic acid (pH 2.5) for 30 min (EMD Millipore, Cat. No. TMS-010-C). Slides were then rinsed in 3% acetic acid and allowed to dry overnight. Slides were cleared in xylene and preserved with Entellan mounting medium (EMD Millipore, Cat. No. 14802) and coverslips. Stained sections were imaged with a Keyence BZ-X700 digital microscope.

Quantification of staining

To quantify the amount of positive staining for CD3ε, B220, Oil Red O, and Alcian blue, we used Fiji (Schindelin et al., 2012). The ‘Colour Deconvolution’ function was used to separate color channels in images of Alcian blue staining. We then converted all stitched images to 8-bit and traced the stroke infarct using the ‘Polygon selections’ tool. We applied a threshold of positive staining to each image and measured the pixel area of positive staining within the selected region. To quantify IgA and CD138, we utilized the ‘Cell Counter’ plugin to manually count the number of positive cells within the stroke infarct. To quantify NeuN and c-Fos immunoreactivity in vehicle- and HPβCD-treated mice, we used Fiji to perform global thresholding in conjunction with a watershed

algorithm on the ipsilateral side and equivalent region in the contralateral hemisphere. Fields covering the selected regions were analyzed at bregma +0.38 mm and −1.46 mm (NeuN) or −1.82 mm (c-Fos) using a 20× objective lens. We also measured hippocampal area in images captured with a 2× objective lens by tracing the hippocampus with the 'Polygon selections' tool in Fiji.

RNA sequencing and data analysis

Fresh brain tissue dissected from vehicle- and HPβCD-treated mice was immersed in RNAlater (Invitrogen, Cat. No. AM7020) and delivered to the University of Arizona Genetics Core. Samples were assessed for quality with an Advanced Analytics Fragment Analyzer (High Sensitivity RNA Analysis Kit, Cat. No. DNF-491/User Guide DNF-491-2014AUG13) and quantity with a Qubit RNA HS Assay Kit (Cat. No. Q32852). Given satisfactory quality (RNA integrity number >8) and quantity, samples were used for library construction with the TruSeq Stranded mRNA Library Prep Kit from Illumina (Cat. No. 20020595), as well as the KAPA Dual-Indexed Adapter Kit from Roche (Cat. No. 8278555702). Upon completion of library construction, samples were assessed for quality and average fragment size with the Advanced Analytics Fragment Analyzer (High Sensitivity NGS Analysis Kit, Cat. No. DNF-846/User Guide DNF-486-2014MAR10). Quantity was assessed with an Illumina Universal Adaptor-specific qPCR kit from KAPA Biosystems (KAPA Library Quantification Kit for Illumina NGS, Cat. No. KK4824/KAPA Library Quantification Technical Guide – AUG2014). Following the final library quality control, samples were equimolar-pooled and clustered for paired-end sequencing on the Illumina NextSeq500 machine to generate 75 bp reads. The

sequencing run was performed using Illumina NextSeq500 run chemistry (NextSeq500/550 High Output v2 Kit 150 cycles, Cat. No. FC-404-2002). Sequencing data is publicly available at the National Center for Biotechnology Information through Gene Expression Omnibus accession numbers: GSE173544 and GSE173715. For data analysis, the resulting sequences were demultiplexed using bcl2fastq v2.19 (Illumina) and trimmed of their indexing adaptors using Trimmomatic v0.32 (Bolger, Lohse, & Usadel, 2014). The trimmed reads were aligned to the GRCm38 reference genome using STAR v2.5.2b (Dobin et al., 2013). Gene expression was calculated using the htseq-count function of the HTSeq python tool (Anders, Pyl, & Huber, 2015). Genes were annotated using the BioMart database. Differential expression analysis of count tables was performed using DESeq2 (Love, Huber, & Anders, 2014). Gene set enrichment analysis (GSEA) was performed on all significant differentially expressed genes (false discovery rate [FDR]-adjusted $p < 0.05$) using a database of Gene Ontology (GO) terms for biological processes. Enrichment maps were constructed from GO terms using the Enrichment Map Cytoscape application (Merico, Isserlin, Stueker, Emili, & Bader, 2010). Minimal editing, such as repositioning of nodes and removal of repetitive gene-sets, was performed to optimize the map layout. Pathway analysis was performed on differentially expressed genes using Ingenuity Pathway Analysis v01-13 (IPA).

Targeted lipidomics analysis (LIPID MAPS Lipidomics Core)

Fresh brain tissue dissected from vehicle- and HPβCD-treated mice was flash frozen and delivered to the LIPID MAPS Lipidomics Core at the University of California, San

298 Diego. Upon arrival, each sample underwent lipid extraction and quality control
299 analyses. The comprehensive sphingolipid panel and cholesterol ester panel were
300 independently performed using established protocols (Quehenberger et al., 2010).
301
302 ***Flow cytometry***
303 To assess peripheral immune cell populations, spleens were extracted after transcardial
304 perfusion with 0.9% saline. Each spleen was crushed in 1 mL ammonium–chloride–
305 potassium RBC lysing buffer and resuspended in 1 mL complete DMEM. For cell
306 staining, fluorophore-conjugated monoclonal antibodies specific for CD4 (RM4-5), CD8α
307 (53-6.7), and TCRβ (H57-597) were obtained from BioLegend. Monoclonal antibodies
308 specific for CD19 (6D5) and GL7 (GL7) were purchased from BD Pharmingen.
309 Antibodies against IgG1 (RMG1-1) and IgA (RMA-1) were obtained from BioLegend.
310 For intranuclear staining, buffers from a Foxp3 Staining Buffer Set (eBioscience) were
311 used to stain antibodies recognizing Foxp3 (FJK-16s, eBioscience). Cells were run on a
312 BD LSR II flow cytometer (BD Biosciences) and analyses were performed with FlowJo
313 v10.7 for Windows (Tree Star).
314
315 ***Y-maze spontaneous alternation behavior test***
316 Spatial working memory was assessed with the spontaneous alternation behavior (SAB)
317 paradigm. Testing occurred in a Y-shaped maze consisting of two symmetrical arms
318 and one longer arm arranged at 120° angles (symmetrical arms: 7.5 cm wide, 37.0 cm
319 long, 12.5 cm high; longer arm: 7.5 cm wide, 42.0 cm long, 12.5 cm high). Mice were
320 placed at the end of the longest arm and allowed to freely explore the three arms in a 5

min trial, as described previously (Doyle et al., 2015). The number of arm entries and the number of correct alternations were recorded by an ANY-maze behavioral video tracking software (Stoelting, Co.). An entry was recorded when all four limbs of the mouse were within an arm.

Light/dark transition test

The light/dark box arena consisted of a Plexiglas box (40 cm wide, 40 cm long, 35 cm high) divided by a small underpass into two equally sized compartments: a brightly illuminated zone (390 lux) and a covered dark zone (2 lux). Prior to the test, animals were habituated to the dark for 30 min. Mice were then placed in the dark chamber of the arena and allowed to move freely between the two chambers for 10 min. The time spent in each chamber, the latency to exit the dark chamber, and the total number of transitions were recorded by an ANY-maze behavioral video tracking software (Stoelting, Co.).

Results

Lipid composition of chronic stroke infarcts in young adult mice

We previously reported that, similar to atherogenesis, chronic stroke infarcts accumulate foamy macrophages, cholesterol crystals, and lipid droplets, which results in the upregulation of osteopontin, MMPs, and pro-inflammatory cytokines (Chung et al., 2018). To further evaluate the similarities between the pathophysiology of chronic stroke infarcts and atherosclerosis, we evaluated lipid droplet accumulation in chronic stroke

infarcts. In the context of atherosclerosis, macrophages frequently become foamy in appearance due to the accumulation of cholesterol esters stored within lipid droplets. In addition to their role as storage containers within foamy macrophages, lipid droplets also contribute directly and indirectly to the pathology of progressing atherosclerotic plaques (Goldberg et al., 2018). To visualize lipid droplets in chronic stroke infarcts, we performed Oil Red O (ORO) staining on brain sections from young adult mice at 7 weeks after stroke. ORO staining revealed more intracellular lipid droplets in infarcts compared to contralateral cortices **(Fig. 1A)**. These findings provide additional evidence that chronic stroke infarcts and atherosclerotic plaques have a similar molecular and morphological profile.

To assess whether lipid accumulation in the infarct results from myelin breakdown following stroke, we performed Alcian blue staining on brain sections from young adult mice at 7 weeks post-stroke. Alcian blue stains for sulfatide, a major constituent of CNS myelin. Importantly, sulfatide was recently identified as a myelin-associated inhibitor of neurite outgrowth (Winzeler et al., 2011). Chronic stroke infarcts contained an abundance of sulfatides at 7 weeks after stroke **(Fig. 1B)**, indicating that phagocytic cells, including resident microglia and infiltrating macrophages, are strained in their capacity to process and eliminate myelin lipid debris for at least 7 weeks after stroke.

To further evaluate myelin-derived lipids in chronic stroke infarcts, we performed targeted lipidomics analysis to assess sphingomyelin levels within infarcts compared to contralateral cortices of young adult mice at 7 weeks after stroke. Importantly,

sphingomyelins play a central role in the structure of myelin, constituting 4% of myelin lipid content. The accumulation of sphingomyelin is a hallmark of Niemann–Pick disease and leads to changes in the plasma membrane that promote neurodegeneration (Mar et al., 2016). Sphingomyelins are also involved in signal transduction pathways and in the regulation of cholesterol and protein trafficking to myelin (Poitelon, Kopec, & Belin, 2020). In addition to their role in myelin architecture, sphingomyelins are involved in microglial activation and inflammation (Fitzner et al., 2020; Yang, Hu, Yang, & Meng, 2020). Chronic stroke infarcts were enriched in sphingomyelins 7 weeks after stroke **(Fig. 1C),** indicating a pronounced dysregulation of myelin lipid homeostasis in chronic stroke infarcts of young adult mice.

Lipid composition of chronic stroke infarcts in aged mice

Stroke remains the leading cause of long-term disability in people over the age of 65 (Virani et al., 2020). Therefore, we used aged (18-month-old) mice to further characterize the lipid composition of chronic stroke infarcts. First, to corroborate our observations in young adult mice, we used ORO to stain for lipid droplets in brain sections collected from aged mice at 7 weeks after stroke. We observed significantly more intracellular lipid droplets in infarcts compared to contralateral cortices **(Fig. 2A)**. In addition, Alcian blue staining revealed that chronic stroke infarcts are characterized by an abundance of sulfatides when compared with contralateral cortices at 7 weeks after stroke **(Fig. 2B)**. When comparing these results with those obtained in young adult mice, we see that aged mice have a comparable accumulation of lipid droplets and sulfatides at 7 weeks after stroke.

Cholesterol is esterified prior to storage in cytoplasmic lipid droplets to prevent free cholesterol-associated cell toxicity (Ghosh, Zhao, Bie, & Song, 2010). Therefore, we evaluated the composition of cholesterol esters stored in lipid droplets via targeted lipidomics analysis. For these analyses, we compared infarcts at 7 weeks after stroke to equivalent regions of the contralateral cortex. All quantified cholesterol ester species were significantly elevated in infarcts of aged mice at 7 weeks after stroke compared to contralateral cortices **(Fig. 2C)**.

Transcriptome of the chronic stroke infarct in young adult mice

To systematically characterize the chronic stroke infarct transcriptome, we conducted bulk RNA sequencing (RNA-Seq) on infarcts collected at 7 weeks after stroke and compared them to equivalent regions of the contralateral cortex **(Fig. 3A)**. As expected, differential expression (DE) analysis revealed marked differences between infarcts and contralateral cortices. The resultant volcano plot illustrates the distribution of 3,930 upregulated and 2,869 downregulated genes **(Fig. 3B)**. The most significantly upregulated genes, including *Lpl*, *Spp1*, *Cd36*, *Mmp2*, and *Mmp19*, and the most highly enriched genes, including *Cd5l*, *Mmp3*, *Mmp12*, and *Mmp13*, indicate a pronounced disturbance in lipid homeostasis in infarcts at 7 weeks after stroke. Importantly, Zhu et al. (2017) similarly identified *Cd5l*, *Lpl*, and *Cd36* as highly expressed genes in foamy macrophages after spinal cord injury (SCI) (Zhu et al., 2017).

412 Correspondingly, chronic stroke infarcts were also characterized by an upregulation of
413 TLRs, including *Tlr1*, *Tlr2*, and *Tlr4*, and scavenger receptors, including *Scarb2*, *Cd68*,
414 *Msr1*, and *Cxcl16*. These genes are implicated in the induction and progression of
415 atherosclerosis; importantly, these scavenger receptors mediate the uptake of oxLDL
416 into macrophages and promote their differentiation into foam cells (Aslanian & Charo,
417 2006; Febbraio, Hajjar, & Silverstein, 2001; Park, 2014; Rahaman et al., 2006; Zeibig et
418 al., 2019). Dysregulated lipid homeostasis within infarcts is further evidenced by the
419 upregulation of genes involved in lipid metabolism: *Npc1*, *Npc2*, *Lamp1*, *Ffar1*, *Pparg*,
420 *Apoe*, *Trem2*, and *Abca1* **(Fig. 3C)**.
421
422 In addition to alterations in lipid metabolism, the transcriptome also revealed a signature
423 of chronic inflammation at 7 weeks after stroke. For instance, activation of the innate
424 immune response is indicated by the upregulation of genes involved in complement
425 cascade activation, including *C1s1*, *C3ar1*, and *C3*, and in phagocytosis, including
426 *Tmem119*, *Hexb*, *Nlrp3*, *Ctsb*, and *Myd88*. Further, upregulated genes included *Gfap*,
427 *Lcn2*, and *Serpina3n*, which have been validated as specific markers of reactive
428 astrogliosis in ischemic stroke and LPS-induced neuroinflammation (Zamanian et al.,
429 2012) **(Fig. 3C)**. Together, these genes signify the activation of innate immune cells,
430 including infiltrating macrophages, resident microglia, and astrocytes.
431
432 Additionally, activation of the adaptive immune system is indicated by the upregulation
433 of genes associated with T lymphocytes, including *Cd2*, *Cd3e*, *Gzma*, *Gzmb*, and *Prf1*;
434 B lymphocytes, including *CD19*, *Cd79a*, and *Blnk*; and antibody-producing plasma cells,

including *Sdc1* and *Jchain* **(Fig. 3C)**. These perturbations in innate and adaptive immunity demonstrate that chronic inflammation persists in infarcts for at least 7 weeks after stroke, as we have shown previously (Chung et al., 2018; Doyle et al., 2015; Zbesko et al., 2020).

In conjunction with the upregulation of genes involved in chronic inflammation and lipid metabolism, the DE analysis revealed a downregulation of genes involved in neuronal structure and function. Specifically, the neurofilament subunits *Nefh*, *Nefm*, and *Nefl* were downregulated, which indicates persistent disruption or absence of neuronal cytoskeletons in infarcts at 7 weeks after stroke **(Fig. 3C)**.

We then used IPA software to define upstream regulators and identify altered biological processes based on DE analysis. Differentially expressed genes were associated with the following upregulated biological processes: (i) atherosclerosis signaling, (ii) IL-1 signaling, (iii) inflammasome pathway, (iv) eicosanoid signaling, (v) B cell receptor (BCR) signaling, and (vi) phospholipases, along with others. In contrast, differentially expressed genes were associated with the following downregulated biological processes: (i) calcium signaling, (ii) glutamate receptor signaling, and (iii) synaptic long-term potentiation **(Fig. 4A, B)**. These altered biological processes indicate that the stroke infarct transcriptome is characterized by chronic inflammation, dysregulated lipid metabolism, and impaired or absent neuronal function at 7 weeks after stroke. In addition, IPA identified lipid metabolic upstream regulators such as cholesterol,

457 phospholipids, and LDL, as well as immunological upstream regulators such as MYD88,
458 IL18, CD3, IL1B, TLR4, and TNF **(Fig. 4C)**.
459
460 ***HPβCD attenuates the chronic inflammatory response to stroke in young adult***
461 ***mice***
462 To investigate the role of lipid metabolism in the chronic inflammatory response to
463 stroke, we administered subcutaneous injections of 4 g/kg HPβCD or vehicle control to
464 young adult mice triweekly (Monday, Wednesday, and Friday) for 6 weeks, beginning 1
465 week after stroke **(Fig. 5A)**. We performed immunostaining on vehicle- and HPβCD-
466 treated brain sections at 7 weeks post-stroke. These analyses revealed substantially
467 fewer B220+ B lymphocytes, CD3ε+ T lymphocytes, and CD138+ and IgA+ antibody-
468 producing plasma cells in infarcts of HPβCD-treated mice than in infarcts of vehicle-
469 injected mice. In addition, ORO staining revealed that infarcts of HPβCD-treated mice
470 had fewer lipid droplets than those of vehicle-injected mice **(Fig. 5B)**. These differences
471 indicate that repeated administration of HPβCD following stroke attenuates chronic
472 inflammation and lipid droplet formation in young adult mice.
473
474 ***HPβCD attenuates the chronic inflammatory response to stroke in aged mice***
475 Stroke prevalence and mortality rates increase with advancing age in both males and
476 females (Virani et al., 2020). Therefore, to address age as a biological variable, we
477 performed immunohistochemistry and bulk RNA-Seq analyses on aged (18-month-old)
478 mice treated with HPβCD using the same treatment regimen as in in young adult mice
479 (HPβCD or vehicle control three times per week for 6 weeks) **(Fig. 6A)**. We discovered

that, consistent with young adult mice, aged mice had substantially fewer B220+ B lymphocytes, CD3ε+ T lymphocytes, and IgA+ antibody-producing plasma cells in infarcts following repeated administration of HPβCD. In addition, ORO staining revealed that infarcts of HPβCD-treated mice had significantly less lipid droplet accumulation than vehicle-injected mice at 7 weeks after stroke **(Fig. 6B)**. When comparing these results with those obtained in young adult mice, we see that aged mice similarly exhibit attenuated lipid droplet and immune cell accumulation in chronic stroke infarcts following repeated administration of HPβCD. Conversely, vehicle- and HPβCD-treated aged mice displayed an equivalent accumulation of sulfatides in chronic stroke infarcts **(Fig. 6B)**, suggesting that HPβCD may not aid in the clearance of sulfatides.

HPβCD does not alter peripheral immune cell populations in the blood or spleens of aged mice after stroke

The spleen, a secondary lymphoid organ, is a major reservoir of immune cells and a focal point for the immune response to tissue injury. In response to ischemic stroke, splenocytes enter into systemic circulation and migrate to the brain, exacerbating neurodegeneration (Seifert et al., 2012). To determine the effect of HPβCD on immune activation at systemic sites, we used flow cytometry to quantify splenic cell populations. There were no significant differences in CD19+ B lymphocytes or GL-7+ germinal center B lymphocytes **(Fig. 7A, B),** or in IgG1 and IgA isotypes **(Fig. 7C)**, between the spleens of vehicle- and HPβCD-treated mice at 7 weeks after stroke. The CD4+ T lymphocyte, CD8+ T lymphocyte, and Treg populations were also not significantly altered by repeated HPβCD administration **(Fig. 7D, E)**. These results demonstrate that

503 splenic cell populations in HPβCD-treated aged mice are not significantly altered in
504 comparison to those of vehicle-injected mice.
505
506 A complete blood count analysis on blood collected from vehicle- and HPβCD-treated
507 aged mice at 7 weeks after stroke revealed no significant differences in the number of
508 circulating white blood cells, neutrophils, lymphocytes, monocytes, eosinophils, or
509 basophils **(Fig. 7F)**. Together, the flow cytometry and complete blood count analyses
510 indicate that, while there were substantially fewer immune cells in infarcts of HPβCD-
511 treated aged mice than in those of vehicle-injected mice at 7 weeks after stroke **(Fig.**
512 **6B)**, repeated systemic HPβCD administration does not significantly alter circulating or
513 splenic immune cell populations in aged mice.
514
515 ***HPβCD promotes lipid metabolism and attenuates inflammation in infarcts of***
516 ***aged mice after stroke***
517 We systematically characterized the transcriptomes of stroke infarcts in vehicle- and
518 HPβCD-treated aged mice by performing bulk RNA-Seq on infarcted brain tissue
519 collected 7 weeks after stroke **(Fig. 8A)**. As shown in the volcano and MA plots, the DE
520 analysis revealed 991 upregulated genes and 1,876 downregulated genes **(Fig. 8B, C)**.
521 HPβCD treatment upregulated intracellular cholesterol transporters, lipoproteins, and
522 lipoprotein receptors, such as *Npc1*, *Npc2*, *Apoe*, *Trem2*, *Abca1*, *Vldlr*, and *Hdlbp*, and
523 downregulated *Ffar1*, *Lrpb1*, and *Dgkb* **(Fig. 8D, E)**. These alterations in lipid
524 metabolism suggest that HPβCD aids in the restoration of lipid homeostasis by 7 weeks
525 after stroke. In addition, the DE analysis revealed a downregulation of genes involved in

526 chemotaxis, including *Cx3cr1*, *Cxcl5*, and *Ccr6*, and innate and adaptive immune
527 responses, including *Mmd2*, *Mzb1*, *Btla*, *Jchain*, and *Igkv5-48*. Correspondingly, there
528 was an upregulation of anti-inflammatory genes, such as *Tgfb1*, *Tgfb2*, *P2ry2*, and
529 *Il18bp* **(Fig. 8D)**. These results indicate that HPβCD attenuates the chronic
530 inflammatory response to stroke in aged mice.
531
532 We also identified alterations in genes involved in the composition of membranes,
533 including *Olig1*, *Pmp22*, *Mal2*, *Rftn1*, and *Plp*. These alterations suggest that HPβCD
534 modifies lipid rafts and cell membranes by 7 weeks after stroke. Genes involved in
535 angiogenesis were also upregulated, including *Nrp1*, *Vash2*, *Hpse*, *Vegfc*, *Vegfd*, and
536 *Ndnf* **(Fig. 8D)**. In addition, enrichment maps constructed from GO terms revealed an
537 upregulation of lipid metabolism, angiogenesis, and collagen synthesis pathways and a
538 downregulation of immune response pathways **(Fig. 9A)**. These results indicate that
539 HPβCD treatment promotes lipid metabolism and angiogenesis and dampens chronic
540 inflammation in infarcts of aged mice at 7 weeks after stroke.
541
542 Next, we performed genome-wide expression analysis of the RNA-Seq data using
543 GSEA, which revealed significant enrichment of various biological processes in infarcts
544 of HPβCD-treated aged mice, including (i) collagen formation, (ii) regulation of
545 angiogenesis, (iii) lipid catabolic process, (iv) regulation of autophagy, and (v) regulation
546 of apoptotic process. Conversely, GSEA identified biological processes more enriched
547 in infarcts of vehicle-injected mice compared to HPβCD-treated mice, including (i) innate
548 immune response, (ii) adaptive immune response, (iii) immunoglobulin production, (iv)

549 phagocytosis, engulfment, and (v) complement activation, classical pathway **(Fig. 9B)**.
550 These results further indicate that infarcts of vehicle-injected mice are defined by
551 increased innate and adaptive immune responses, whereas those of HPβCD-treated
552 mice are defined by increased angiogenic and lipid metabolic processes.
553
554 ***Transcriptome of the peri-infarct region in aged mice at 7 weeks after stroke***
555 Prior to assessing the impact of repeated HPβCD administration on the peri-infarct
556 region of the brain, we first compared the transcriptome of the peri-infarct region to the
557 equivalent region of the contralateral hemisphere in aged mice at 7 weeks after stroke
558 **(Fig. 10A)**. The peri-infarct region was characterized by 3,910 differentially expressed
559 genes **(Fig. 10B, C)**. Of these, 2,123 were upregulated, many of which were also
560 upregulated in infarcts at 7 weeks after stroke **(Fig. 3C)**. For instance, the infarct and
561 peri-infarct regions were both defined by the upregulation of degradative enzymes,
562 including *Mmp2*, *Mmp3*, and *Mmp8*; TLRs, including *Tlr1*, *Tlr2*, and *Tlr4*; and scavenger
563 receptors, including *Cd36*, *Cd68*, and *Cxcl16*. Additionally, peri-infarct regions were
564 characterized by specific markers of reactive astrogliosis, including *Gfap*, *Lcn2*, and
565 *Serpina3n* **(Fig. 10D)**.
566
567 Similar to the transcriptome of the infarct at 7 weeks after stroke, the transcriptome of
568 the peri-infarct region was primarily defined by genes involved in chronic inflammation
569 and dysregulated lipid metabolism. The upregulation of *Lpl*, *Lrp2*, *Ch25h*, *Apoe*, *Trem2*,
570 and *Abca1* signifies a divergence from lipid homeostasis. Moreover, *Ldlr* was
571 downregulated, which implies impaired lipoprotein and lipid metabolism (Go & Mani,

572 2012). In addition, genes involved in complement cascade activation (including *C1s1*,
573 *C3ar1*, and *C3*) and phagocytosis (including *Tmem119*, *Hexb*, *Nlrp3*, and *Mmd2*) were
574 upregulated in peri-infarct regions. These alterations in innate immunity coincided with
575 corresponding perturbations in adaptive immunity. The upregulation of *Cd3d*, *Cd3e*,
576 *Cd3g*, *Blnk*, *Sdc1* and *Jchain* suggests that chronic inflammation persists in peri-infarct
577 regions for at least 7 weeks after stroke **(Fig. 10D)**.
578
579 Conversely, the DE analysis revealed that 1,787 genes were downregulated in peri-
580 infarct regions compared to equivalent regions of the contralateral hemisphere. These
581 genes were primarily involved in mitochondrial respiration and neuronal function.
582 Specifically, genes involved in mitochondrial fission and respiration, including *Cyc1*,
583 *Coa3*, *Cox5a*, and *Mff*, and the neurofilament subunits *Nefh*, *Nefm*, and *Nefl*, were
584 downregulated **(Fig. 10D)**. Together, these results demonstrate that the transcriptome
585 of the peri-infarct region is characterized by the upregulation of genes involved in
586 inflammation and lipid metabolism and the downregulation of genes involved in
587 mitochondrial respiration and neuronal function.
588
589 Next, we performed genome-wide expression analysis of the RNA-Seq data using
590 GSEA. GSEA revealed significant enrichment of various biological processes in peri-
591 infarct regions of aged mice, including (i) macrophage activation, (ii) cytokine
592 production, (iii) BCR signaling pathway, (iv) lipoprotein metabolism, and (v)
593 phagocytosis. In contrast, GSEA identified biological processes more significantly
594 enriched in equivalent regions of the contralateral hemisphere, including (i) synaptic

595 vesicle localization, (ii) mitochondrion organization, (iii) neurotransmitter secretion, (iv)
596 myelin sheath, and (v) mitochondrial transport **(Fig. 11)**. These results further indicate
597 that peri-infarct regions are defined by chronic inflammation and dysregulated lipid
598 metabolism, whereas equivalent regions of the contralateral hemisphere are defined by
599 intact neuronal function.
600
601 ***HPβCD attenuates inflammation and increases transcripts associated with***
602 ***neuronal function in peri-infarct regions of aged mice after stroke***
603 To evaluate the impact of HPβCD treatment on the transcriptome of the peri-infarct
604 region, we performed bulk RNA-Seq on brain tissue collected 7 weeks after stroke. For
605 this analysis, we compared the peri-infarct regions of vehicle- and HPβCD-treated aged
606 mice **(Fig. 12A)**. The peri-infarct region of HPβCD-treated mice was characterized by
607 5,385 differentially expressed genes **(Fig. 12B, C)**. The DE analysis revealed that
608 specific markers of reactive astrogliosis, including *Gfap*, *Serpina3n*, and *Stat3*, were
609 downregulated following HPβCD treatment. The peri-infarct region of HPβCD-treated
610 mice was also characterized by the downregulation of multiple degradative enzymes,
611 including *Mmp2*, *Mmp8*, and *Mmp14*; chemokine receptors, including *Ccr2*, *Cx3cr1*; and
612 *Cxcr4*, and scavenger receptors, including *Cd36*, *Cd68*, and *Cxcl16* **(Fig. 12D)**.
613
614 In addition, the transcriptomic analysis demonstrated a restoration of lipid homeostasis
615 in peri-infarct regions of HPβCD-treated mice compared to vehicle-injected mice, as
616 evidenced by the downregulation of *Lipa*, *Apoe*, *Lamp1*, *Npc1*, and *Npc2* and
617 upregulation of *Nceh1* and *Ldlr*. A reduction in the innate immune response (identified

by *Tlr4*, *Csf1*, and *C2*) and in the adaptive immune response (identified by *Sdc1*, *Gsdmd*, and *Cd1d1*) characterized peri-infarct regions of HPβCD-treated mice **(Fig. 12D)**; these alterations are consistent with the attenuated chronic inflammation that characterized infarcts of the HPβCD-treated aged mice **(Fig. 8D)**. These results demonstrate that HPβCD treatment after stroke attenuates chronic inflammation and promotes lipid metabolism in peri-infarct regions of aged mice. Additionally, the DE analysis revealed an upregulation of genes involved in myelin sheath structural integrity, such as *Ina*, *Omg*, and *Nefl*, and synaptic plasticity and neuroplasticity, such as *Syn1*, *Bdnf*, *Nrg1*, *Negr1*, and *Nsg1* **(Fig. 12D)**. These results suggest that HPβCD treatment improves the structure and function of neurons in peri-infarct regions of aged mice after stroke.

Next, we performed genome-wide expression analysis of the RNA-Seq data using GSEA, which revealed a significant enrichment of various biological processes in peri-infarct regions of HPβCD-treated aged mice, including (i) synaptic vesicle localization, (ii) neuron projection membrane, (iii) dendritic spine organization, (iv) myelin sheath, and (v) regulation of axonogenesis. Conversely, biological processes more significantly enriched in vehicle-injected mice than in HPβCD-treated mice included (i) macrophage activation, (ii) binding and uptake of ligands by scavenger receptors, (iii) cytokine production, (iv) lipid droplet, (v) lymphocyte mediated immunity, and (vi) lipid catabolic process **(Fig. 13)**. These results demonstrate that peri-infarct regions of HPβCD-treated aged mice are characterized by enhanced membrane integrity and reduced inflammation compared to vehicle-injected aged mice.

HPβCD attenuates neurodegeneration and improves recovery in aged mice after stroke

To assess behavioral outcomes following HPβCD treatment, we used the light/dark transition test and the Y-maze spontaneous alternation behavior (SAB) test. The light/dark transition test is based on the innate aversion of mice to brightly illuminated areas and on their spontaneous exploratory behavior in response to mild stressors (Bourin & Hascoët, 2003; Takao & Miyakawa, 2006). Our results revealed that in the light/dark box, HPβCD-treated mice spent less time in the brightly illuminated compartment than vehicle-injected mice **(Fig. 14A)**. Additionally, HPβCD-treated mice were slower to emerge from the dark compartment after being habituated to the dark for 30 min prior to the test **(Fig. 14A)**. These behaviors indicate decreased impulsivity and behavioral disinhibition in HPβCD-treated mice. We also assessed hippocampal-dependent spatial working memory at 7 weeks after stroke with the Y-maze SAB test (Yamada et al., 1996). We discovered that vehicle-injected mice developed a delayed cognitive deficit, whereas HPβCD-treated mice displayed neurotypical cognitive function comparable to baseline recordings **(Fig. 14B)**. To assess hippocampal edema, we measured the total hippocampal area of the ipsilateral and contralateral hemispheres in aged mice that received vehicle or HPβCD. Hippocampal enlargement 7 weeks after stroke was attenuated in mice that had received HPβCD **(Fig. 14C)**. This reduction in hippocampal edema correlates with improved hippocampal-dependent spatial working memory outcomes in the Y-maze SAB test **(Fig. 14B)**. We next evaluated secondary neurodegeneration by quantifying NeuN immunoreactivity as a biomarker of secondary

664 neurodegeneration in regions of axonal degeneration. Repeated administration of
665 HPβCD led to the preservation of NeuN immunoreactivity in the striatum and thalamus
666 **(Fig. 14D, E)**. These results demonstrate that HPβCD attenuates secondary
667 neurodegeneration and improves cognitive function following stroke.
668
669 To investigate neuronal activation in hippocampal regions, we next measured the
670 immunoreactivity of c-Fos, a transcription factor thought to primarily reflect NMDA-
671 mediated neuronal activity (Albertini et al., 2018). We observed an induction of c-Fos
672 expression in the dentate gyrus, CA1, and CA3 areas of HPβCD-treated mice **(Fig.**
673 **14F)**. Importantly, Fleischmann et al. demonstrated a critical role for c-Fos in
674 hippocampal-dependent spatial learning and memory, as well as in NMDA receptor-
675 dependent LTP formation (Fleischmann et al., 2003). Together, our results show that
676 improvement in hippocampal-dependent spatial working memory **(Fig. 14B)** correlates
677 with an induction of c-Fos in hippocampal regions of HPβCD-treated mice at 7 weeks
678 after stroke.
679
680 To corroborate these findings, we further analyzed the results from the GSEA
681 performed on peri-infarct regions from vehicle- and HPβCD-treated aged mice **(Fig. 13)**.
682 We discovered that peri-infarct regions of HPβCD-treated aged mice were characterized
683 by enriched biological processes that signify improved neuronal and synaptic function,
684 including (i) long-term synaptic potentiation, (ii) neurotransmitter transport, (iii) synaptic
685 signaling, (iv) glutamate receptor activity, (v) membrane depolarization during action

686 potential, and (vi) learning or memory **(Fig. 14G)**. These results provide evidence that
687 HPβCD improves neuronal integrity in peri-infarct regions by 7 weeks after stroke.
688
689 **Discussion (1,500 words maximum, including citations)**
690
691 Dysregulated lipid homeostasis has been implicated in chronic neurodegenerative
692 diseases, including Alzheimer's disease, Parkinson's disease, and Niemann–Pick
693 disease type C, and in acute neuronal injuries, including ischemic stroke (Vance, 2012).
694 Lipid metabolism is particularly important in the mammalian brain, as lipids constitute
695 50–60% of the dry weight (Luchtman & Song, 2013). Notably, the mammalian brain is
696 highly enriched in cholesterol, which primarily exists in two distinct pools within the
697 CNS: in plasma membranes of glial cells and neurons and in myelin sheaths
698 surrounding axons. Due to the intact blood–brain barrier, cholesterol synthesis and
699 lipoprotein transport are regulated independently of the peripheral circulation (Dietschy
700 & Turley, 2001; Vance, 2012). Therefore, further investigation into the role of altered
701 lipid metabolism in neurodegeneration will likely aid in the development of novel
702 therapeutic strategies.
703
704 Our preclinical studies indicate that the pathological characteristics of chronic stroke
705 infarcts closely resemble the hallmark features of atherosclerotic plaques. Similar to
706 atherosclerotic plaques, chronic stroke infarcts contain foamy macrophages, lipid
707 droplets, and intracellular and extracellular cholesterol crystals (Chung et al., 2018). We
708 have also shown that the development of these pathologies coincides with the

recruitment and infiltration of adaptive immune cells (Doyle et al., 2015; Zbesko et al., 2020). Importantly, in atherogenesis, the formation of foamy macrophages, caused by dysregulated lipid metabolic processes, leads to the recruitment of adaptive immune cells and the production of cytokines and degradative enzymes. Herein, we postulated that following stroke, lipids derived from myelin debris and other cell membranes overwhelm the processing capability of phagocytes in the brain, leading to the formation of lipid-laden foam cells, generation of cholesterol crystals, secretion of pro-inflammatory cytokines, and production of degradative enzymes. Further, we hypothesized that this chronic inflammatory response, coupled with concurrent cell death, causes post-stroke secondary neurodegeneration and impairs functional recovery.

Using the distal middle cerebral artery occlusion + hypoxia mouse model of stroke, we first characterized the lipidome of chronic stroke infarcts. The lipidome of infarcts at 7 weeks after stroke showed a substantial elevation of lipids, including sphingomyelins, sulfatides, and cholesterol esters, compared to contralateral cortices. We also observed an accumulation of intracellular lipid droplets. It has been shown that the excessive accumulation of cholesterol esters in lipid droplets contributes to foam cell formation (Yu, Fu, Zhang, Yin, & Tang, 2013). Therefore, the foam cells identified in chronic stroke infarcts likely contain an abundance of myelin-derived lipids.

Using transcriptomic analyses, we assessed the impact of lipid dyshomeostasis on chronic stroke infarcts and peri-infarct regions. We anticipated disparity between

ipsilateral and contralateral regions. Indeed, the transcriptomes of chronic stroke infarcts and peri-infarct regions were characterized by an upregulation of genes involved in inflammation, reactive astrogliosis, and lipid metabolism. Specifically, the upregulation of TLRs, including *Tlr1*, *Tlr2*, and *Tlr4*; scavenger receptors, including *Scarb2*, *Cd68*, *Msr1*, and *Cxcl16*; and other lipid mediators, including *Npc1*, *Npc2*, *Lamp1*, *Ffar1*, *Pparg*, *Apoe*, *Trem2*, and *Abca1* indicates a pronounced disruption in lipid homeostasis at 7 weeks after stroke. These transcriptomic analyses suggest that the mechanism of foam cell formation in ischemic stroke shares commonalities with the mechanism extensively characterized in atherosclerosis, albeit distinct in that myelin debris, rather than circulating LDL cholesterol, is the primary source of lipids that overwhelm the processing capacity of infiltrating macrophages and resident microglia.

We next assessed the efficacy of HPβCD in counteracting or reversing foam cell formation and immune cell infiltration following stroke, as HPβCD induces liver X receptor target gene expression in macrophages and leads to an increase in cholesterol transporters that further promote cholesterol efflux (Zimmer et al., 2016). Cyclodextrins are cyclic oligosaccharides comprised of glucose monomers. With hydrophobic interiors and hydrophilic exteriors, cyclodextrins can form inclusion complexes with hydrophobic compounds and yield aqueous solubility and stability across tissues. Cyclodextrins are commonly utilized as carriers and solubilizing agents for steroids, antivirals, and chemotherapies (Gidwani & Vyas, 2015; Rasheed, Kumar C.K., & Sravanthi, 2008). In addition, HPβCD has also proven efficacious in the regression of atherosclerotic plaques and the prevention of age-related lipofuscin accumulation (Gaspar et al., 2017;

Zimmer et al., 2016). Here, we found that repeated administration of HPβCD after stroke significantly attenuated chronic inflammation in young adult and aged mouse models. Specifically, there were substantially fewer intracellular lipid droplets, B lymphocytes, T lymphocytes, and antibody-producing plasma cells in the infarcts of young adult and aged HPβCD-treated mice than in vehicle-injected mice at 7 weeks after stroke.

We discovered that HPβCD is effective in attenuating B-lymphocyte accumulation in chronic stroke infarcts, which suggests that HPβCD has potential as a treatment for post-stroke dementia. We have shown that B lymphocytes mediate cognitive dysfunction following stroke (Doyle et al., 2015). Correspondingly, activated B lymphocytes and autoantibodies have been shown to cause neuropathology in models of experimental autoimmune encephalomyelitis (EAE), SCI, and transient middle cerebral artery occlusion (Ankeny, Lucin, Sanders, McGaughy, & Popovich, 2006; Ortega et al., 2015; Raine, Cannella, Hauser, & Genain, 1999). Recently, we also found that the production of natural IgA antibodies is a part of the B-lymphocyte response to stroke (Zbesko et al., 2020). However, future studies are required to determine if the function of these natural IgA antibodies is to aid in the clearance of myelin debris and the neutralization of apoptotic foamy macrophages.

Using transcriptomic analyses, we next assessed transcripts in infarct and peri-infarct regions of HPβCD-treated aged mice. We found that systemic administration of HPβCD distinctively altered the transcriptomes of infarct and peri-infarct regions. In infarcts,

778 HPβCD upregulated genes involved in lipid metabolic processes, including *Lipa*, *Npc1*,
779 *Apoe*, and *Abca1*; in peri-infarct regions, HPβCD had an inverse effect on these genes.
780 These observations suggest that HPβCD has supported the restoration of lipid
781 homeostasis through transcriptional reprogramming of macrophages, consistent with a
782 previously described mechanism of action (Zimmer et al., 2016). In addition, HPβCD
783 influenced expression profiles in infarcts through the upregulation of genes involved in
784 angiogenesis and in peri-infarct regions through the upregulation of genes involved in
785 neuronal and synaptic structure and function. Together, these results indicate that
786 HPβCD exerts multiple restorative effects on affected brain regions after stroke.
787
788 We next evaluated the efficacy of HPβCD in enhancing recovery after stroke. We
789 assessed impulsivity and risk-taking behavior using the light/dark transition test. We
790 have previously demonstrated a chronic impact of stroke on the psychological
791 measurement of impulsivity in the light/dark transition test, resembling the uninhibited,
792 risk-taking behaviors exhibited by patients with Alzheimer and frontotemporal dementias
793 (Liscic, Storandt, Cairns, & Morris, 2007; Nguyen et al., 2018). HPβCD-treated mice
794 spent less time in the brightly illuminated chamber and were slower to exit the dark
795 chamber. These behaviors suggest that HPβCD-treated mice act less erratically and
796 impulsively than vehicle-injected mice. We also measured hippocampal-dependent
797 spatial working memory using the Y-maze spontaneous alternation behavior test. We
798 found that vehicle-injected mice developed a delayed cognitive deficit, whereas HPβCD-
799 treated mice displayed neurotypical cognitive function. This improvement in recovery
800 correlated with a reduction in hippocampal edema, a preservation of neurons in the

striatum and thalamus, and an induction of c-Fos expression in hippocampal regions (dentate gyrus, CA1, CA3). Correspondingly, peri-infarct regions of HPβCD-treated mice were defined by an enrichment of biological processes signifying improved neuronal and synaptic integrity. Thus, administration of HPβCD reduced stroke-induced neuropathology and improved cognitive function after stroke.

In conclusion, we have shown that, coincident with the progressive infiltration of adaptive immune cells, chronic stroke infarcts accumulate lipids, including sphingomyelins, sulfatides, and cholesterol esters. To our knowledge, this substantial disruption in lipid homeostasis has not been previously recognized or investigated in the context of stroke. We also discovered that repeated administration of HPβCD following stroke aids in the restoration of lipid homeostasis, attenuates lipid droplet and immune cell accumulation, and improves recovery at transcriptional and functional levels. Therefore, we propose that HPβCD could be repurposed for the treatment of ischemic stroke and other CNS injuries.

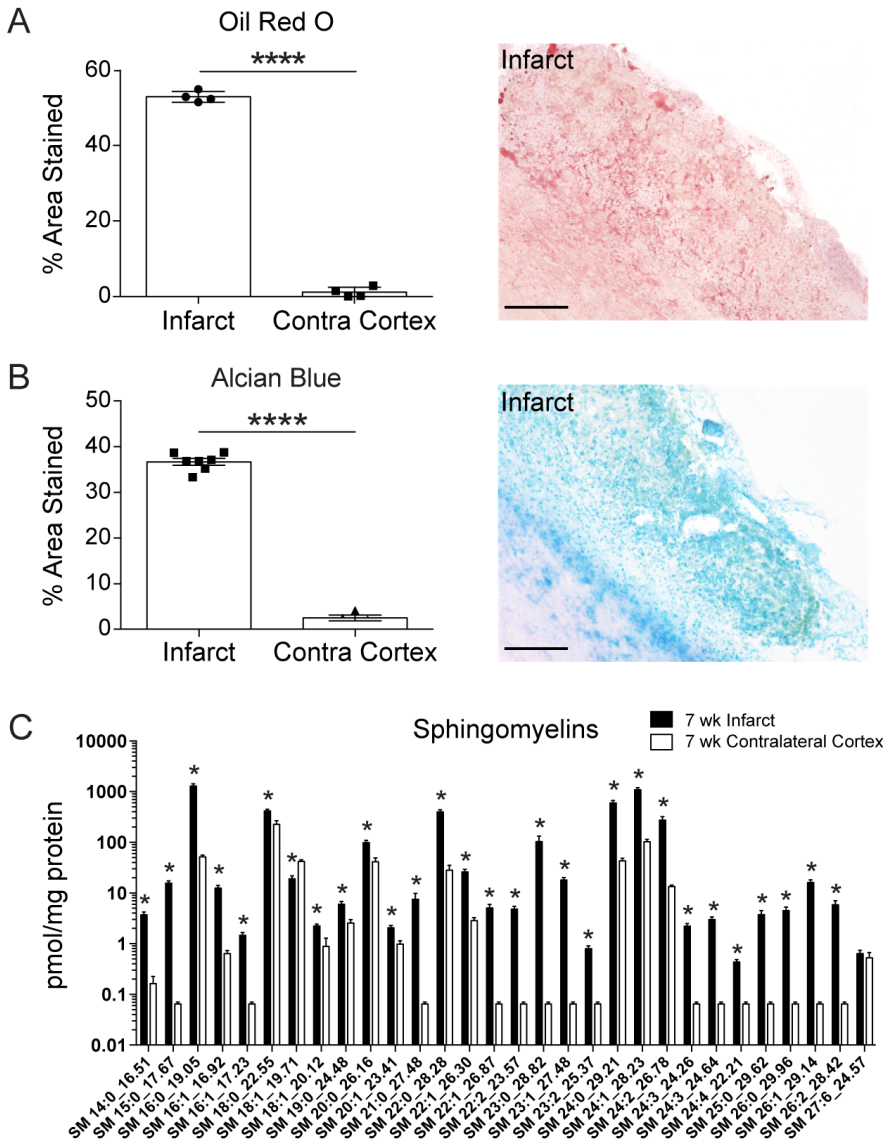

Figure 1. Lipid composition of chronic stroke infarcts in young adult mice. ***A, B,*** Representative 20× images and quantification of positive staining with Oil Red O (***A***) and Alcian blue (***B***) show markedly more lipid droplets and sulfatides, respectively, in infarcts than in contralateral cortices. Scale bar, 125 μm. ($n \geq 4$; paired (***A***) or unpaired (***B***) *t* test; ****$p < 0.0001$). ***C,*** Targeted lipidomics analysis revealed that infarcts had significantly higher levels of sphingomyelins than equivalent regions of the contralateral

823 cortex at 7 weeks after stroke. (n = 8; multiple t tests, Holm–Sidak correction for multiple

824 comparisons; *p < 0.05). Data are presented as mean ± SEM.

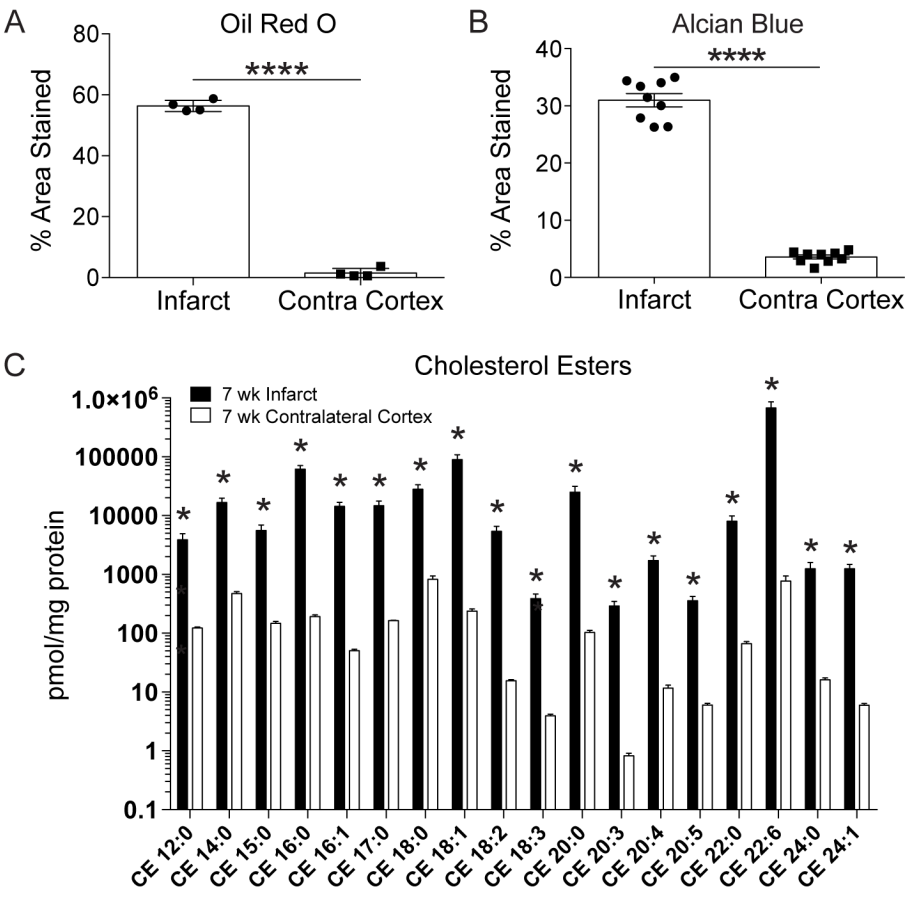

Figure 2. Lipid composition of chronic stroke infarcts in aged mice. *A, B,* Quantification of positive staining with Oil Red O (***A***) and Alcian blue (***B***) shows significantly more lipid droplets and sulfatides, respectively, in infarcts compared to contralateral cortices. Scale bar, 125 μm. ($n \geq 4$; paired *t* tests; ****$p < 0.0001$). ***C,*** Targeted lipidomics analysis revealed significantly higher levels of cholesterol esters in infarcts than in equivalent regions of the contralateral cortex at 7 weeks after stroke. ($n = 5$; multiple *t* tests, Holm–Sidak correction for multiple comparisons; *$p < 0.05$). Data are presented as mean ± SEM. CE, cholesterol ester.

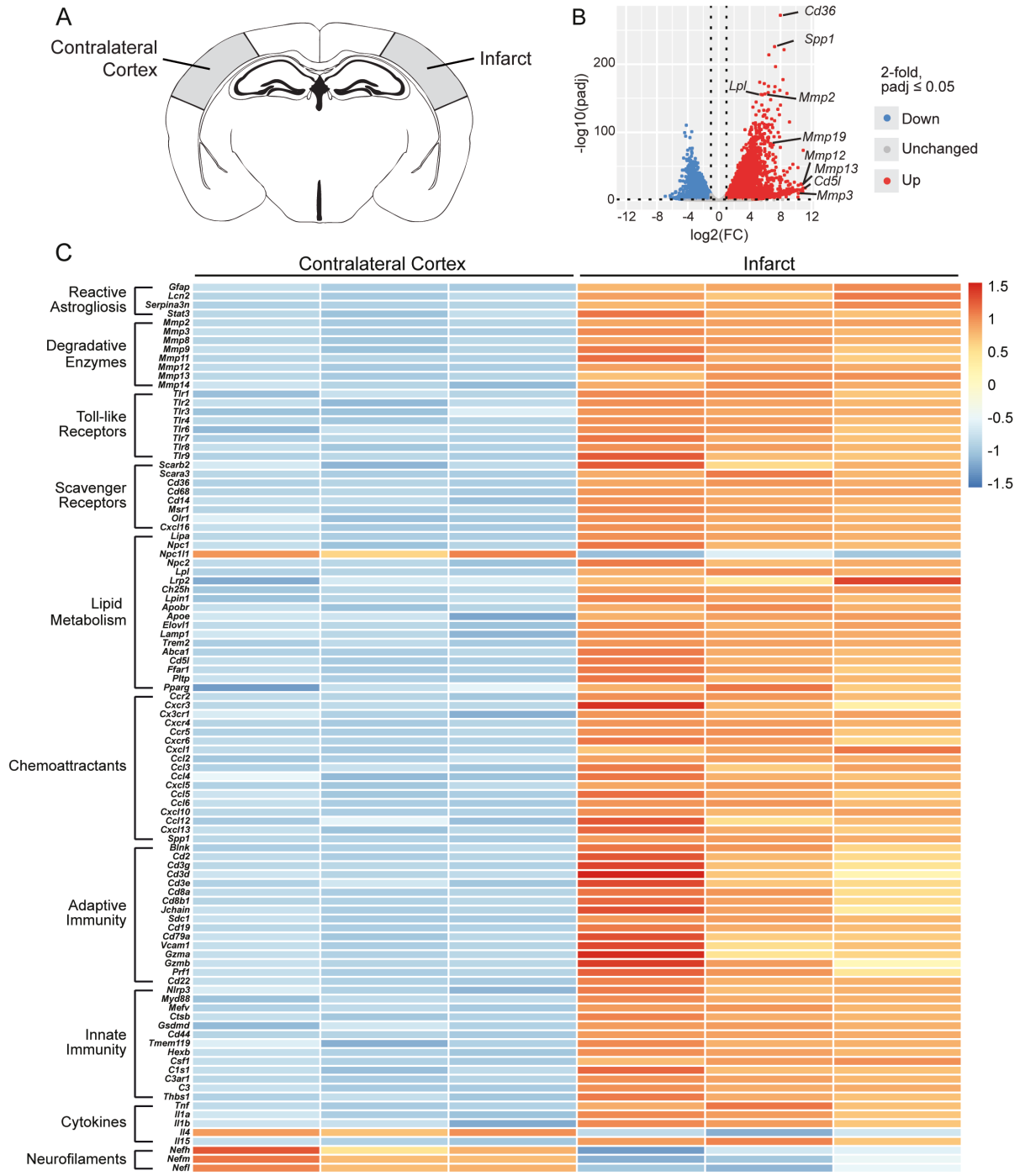

Figure 3. Transcriptome of the chronic stroke infarct in young adult mice. *A,* Schematic of a mouse coronal brain section following stroke induced by distal middle cerebral artery occlusion + hypoxia, with the analyzed region of each hemisphere

838 shaded in gray. ***B,*** Volcano plot showing differences in gene expression between the
839 infarct and contralateral cortex at 7 weeks following stroke (false discovery rate-
840 adjusted $p < 0.05$; FC > |2|). ***C,*** Row-scaled heatmap displaying differentially expressed
841 genes associated with dysregulated lipid metabolism and pronounced inflammation
842 (false discovery rate-adjusted $p < 0.05$; FC > |2|). FC, fold change.

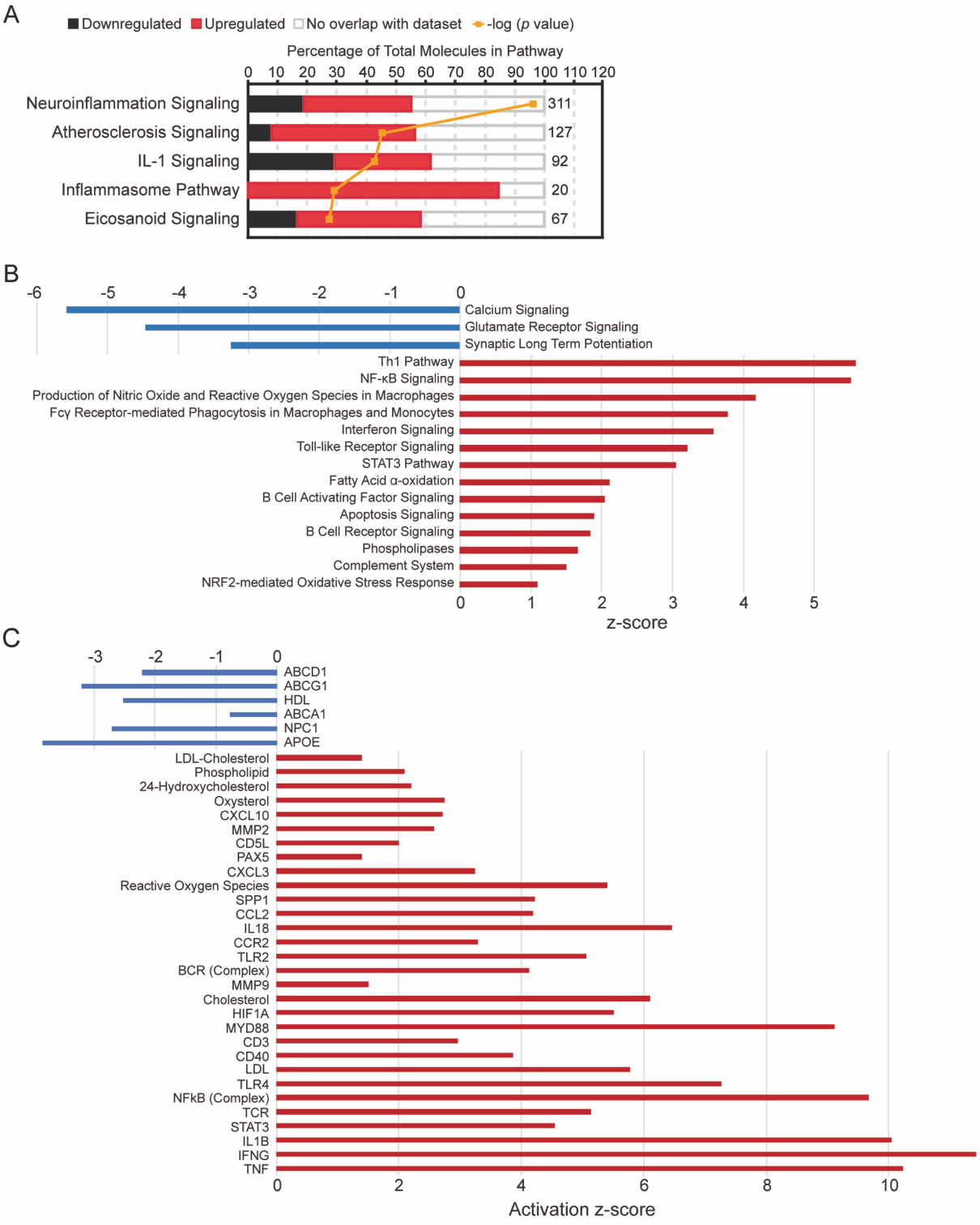

Figure 4. Canonical pathways and upstream regulators based on differentially expressed genes in chronic stroke infarcts of young adult mice. *A,* Ingenuity

Pathway Analysis (IPA) performed on differentially expressed genes revealed a significant upregulation of inflammatory pathways in infarcts of young adult mice at 7 weeks after stroke compared to contralateral cortices. ***B,*** Additional canonical pathway analysis confirmed activation of inflammatory pathways in the infarcts of young adult mice at 7 weeks after stroke. ***C,*** IPA identified putative upstream regulators associated with inflammation and lipid metabolism, including cholesterol, LDL, MYD88, CD3, and IL1B. All canonical pathways and upstream regulators shown are significantly up- or downregulated ($p < 0.05$).

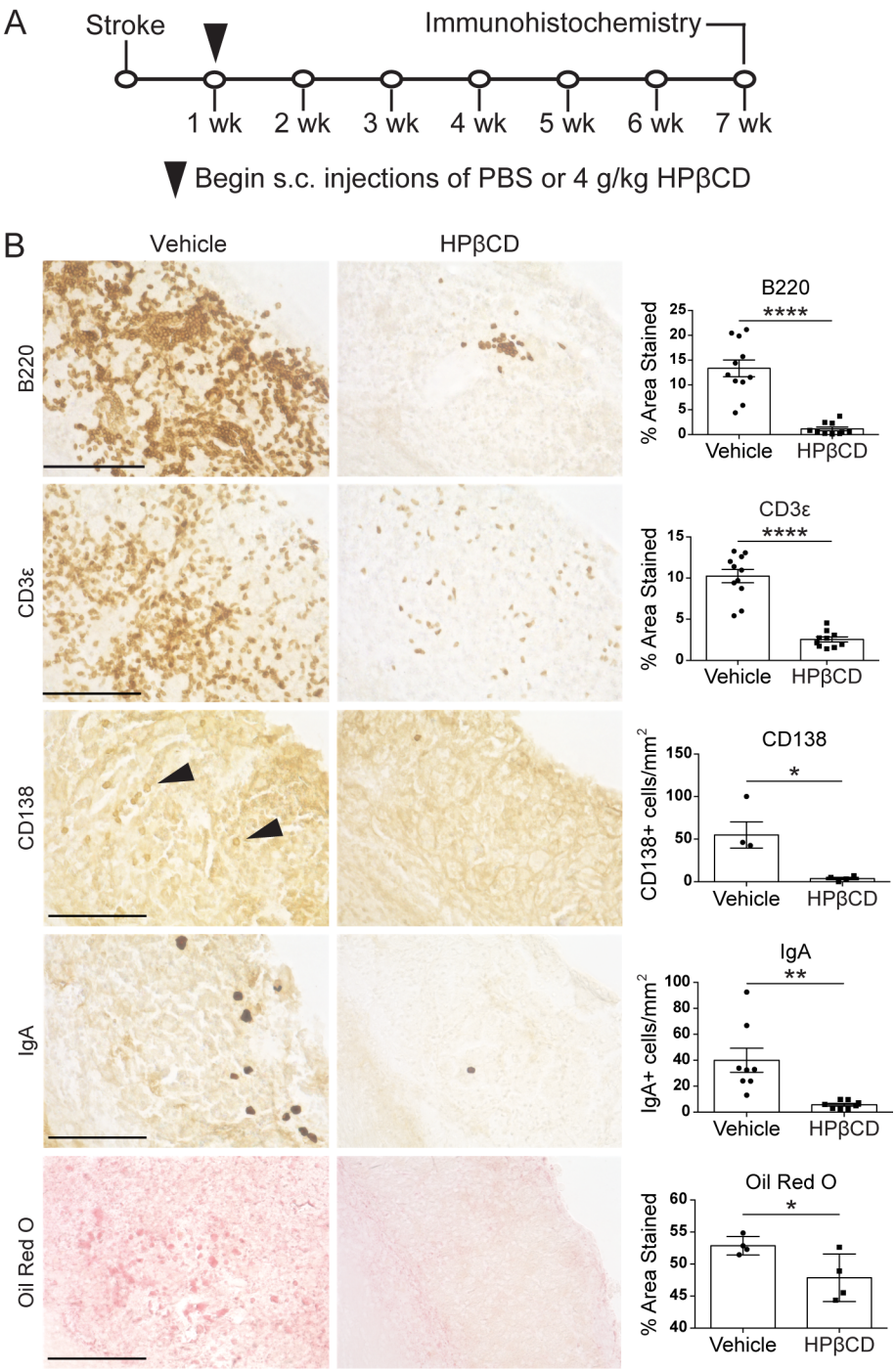

Figure 5. HPβCD attenuates the chronic inflammatory response to stroke in young adult mice. ***A,*** Experimental design, *n* = 31–32 per group. Three-month-old mice received subcutaneous (s.c.) injections of 4 g/kg HPβCD or vehicle three times a

week, beginning 1 week after stroke induced by distal middle cerebral artery occlusion + hypoxia. Brains were extracted at 7 weeks post-stroke and processed for immunohistochemistry. ***B,*** Representative 40× images of infarcts in vehicle- or HPβCD-treated young adult mice stained for B lymphocytes (B220), T lymphocytes (CD3ε), antibody-producing plasma cells (CD138, IgA) and lipid droplets (Oil Red O). Quantification of images is shown to the right of each photomicrograph. (n = 4–11; unpaired t tests; *p < 0.05, **p < 0.01, ****p < 0.0001). Scale bar, 125 μm. Data are presented as mean ± SEM.

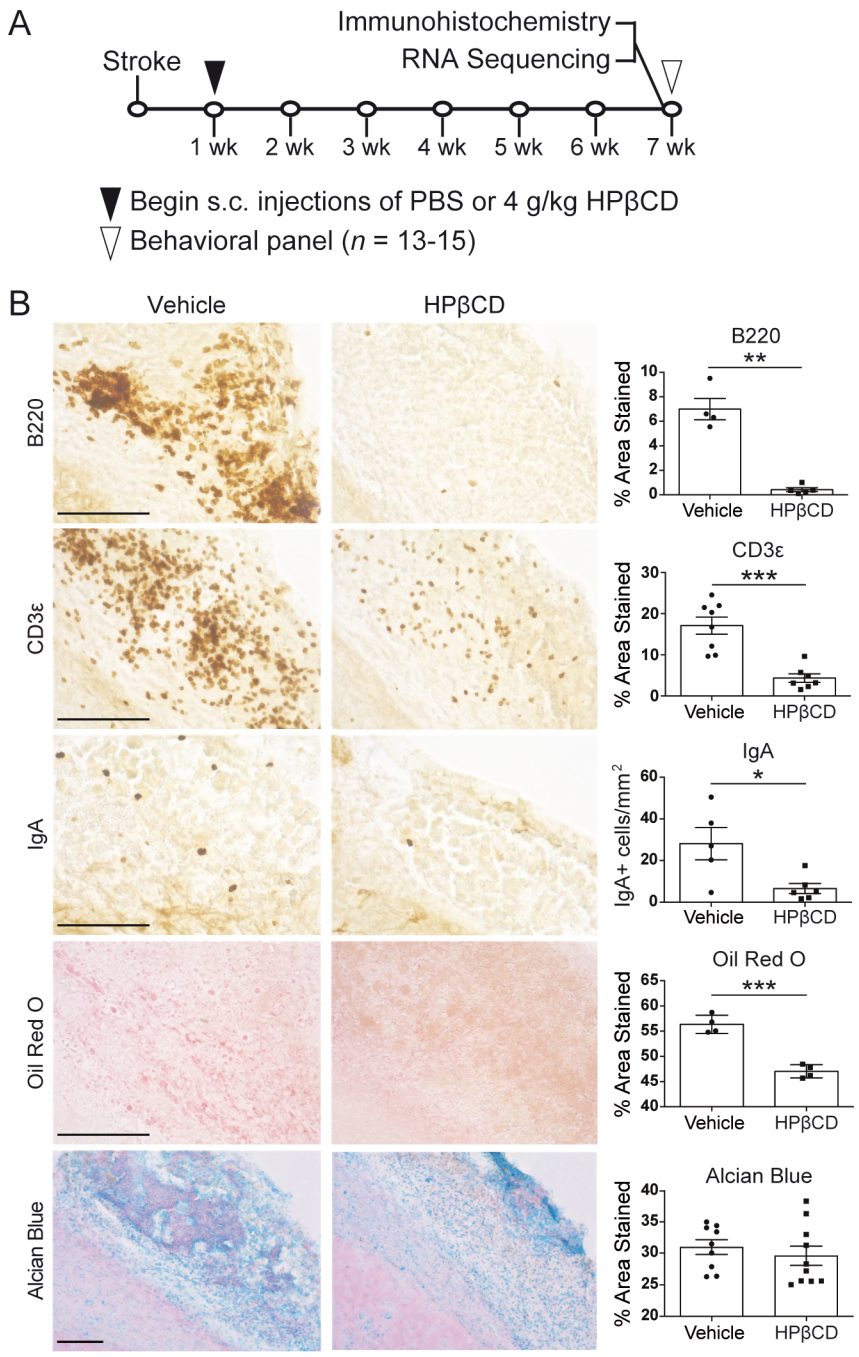

Figure 6. HPβCD attenuates the chronic inflammatory response to stroke in aged mice. ***A,*** Experimental design, *n* = 39–40 per group. Eighteen-month-old mice received subcutaneous (s.c.) injections of 4 g/kg HPβCD or vehicle three times a week, beginning 1 week after stroke induced by distal middle cerebral artery occlusion +

hypoxia. Brains were dissected at 7 weeks post-stroke and processed for immunohistochemistry or RNA-Seq. ***B,*** Representative 40× images of infarcts in vehicle- or HPβCD-treated aged mice stained for B lymphocytes (B220), T lymphocytes (CD3ε), antibody-producing plasma cells (IgA), and lipid droplets (Oil Red O), followed by representative 20× images of infarcts stained for sulfatides (Alcian Blue). Quantification of images is shown to the right of each photomicrograph. (n = 4–10; unpaired t tests; *p < 0.05, **p < 0.01, ***p < 0.001). Scale bar, 125 μm. Data are presented as mean ± SEM.

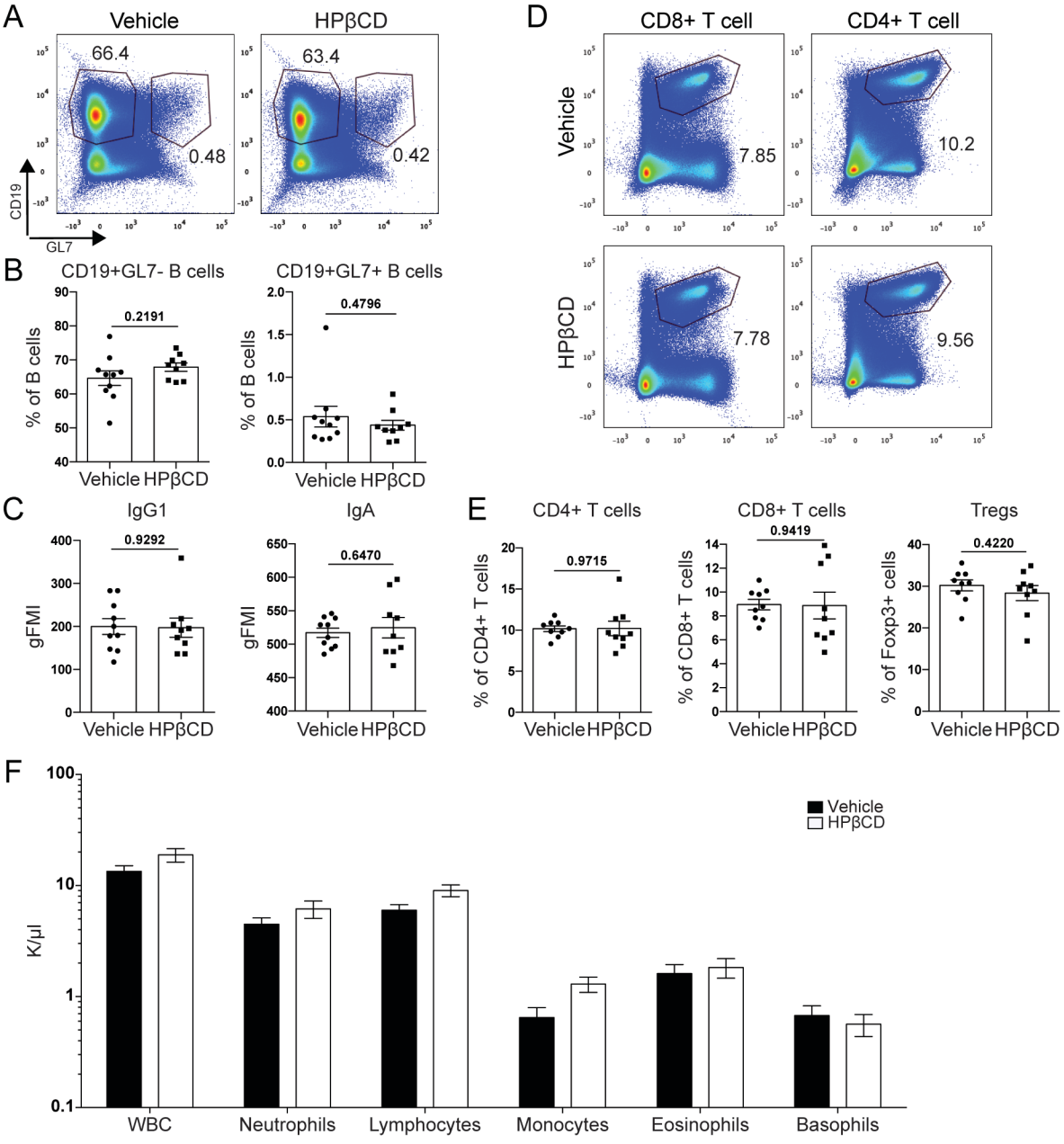

Figure 7. HPβCD does not alter peripheral immune cell populations in the blood or spleens of aged mice after stroke. ***A, B,*** Splenocytes from HPβCD- and vehicle-injected aged mice were stained with antibodies against CD19 and GL7. Representative flow cytometry plots (***A***) and quantification of CD19+GL7- B cells and CD19+GL7+ germinal center B cells as a percentage of total lymphocytes (***B***) showed no significant

differences in splenic B cell populations between vehicle- and HPβCD-treated aged mice at 7 weeks after stroke. ***C,*** Quantification of antibody isotypes (IgG1 and IgA) in the spleen revealed no significant differences between vehicle- and HPβCD-treated aged mice at 7 weeks after stroke. ***D, E,*** Splenocytes from HPβCD- and vehicle-injected aged mice were stained with antibodies against TCRβ, CD4, CD8, and Foxp3. Representative flow cytometry plots of CD4+ and CD8+ T cells (***D***) and quantification of CD4+ T cells, CD8+ T cells, and Tregs as a percentage of total lymphocytes (for CD4+ and CD8+ gates) or TCRβ+CD4+ T cells (for Treg gate) (***E***) revealed no significant differences in splenic T cell populations between vehicle- and HPβCD-treated aged mice at 7 weeks after stroke. (n = 9–10; unpaired t tests; *$p < 0.05$). ***F,*** Complete blood count analysis in vehicle- and HPβCD-treated aged mice at 7 weeks after stroke revealed no significant differences in circulating immune cell populations (n = 6; multiple t tests, Holm–Sidak correction for multiple comparisons; *$p < 0.05$). Data are presented as mean ± SEM. GC, germinal center.

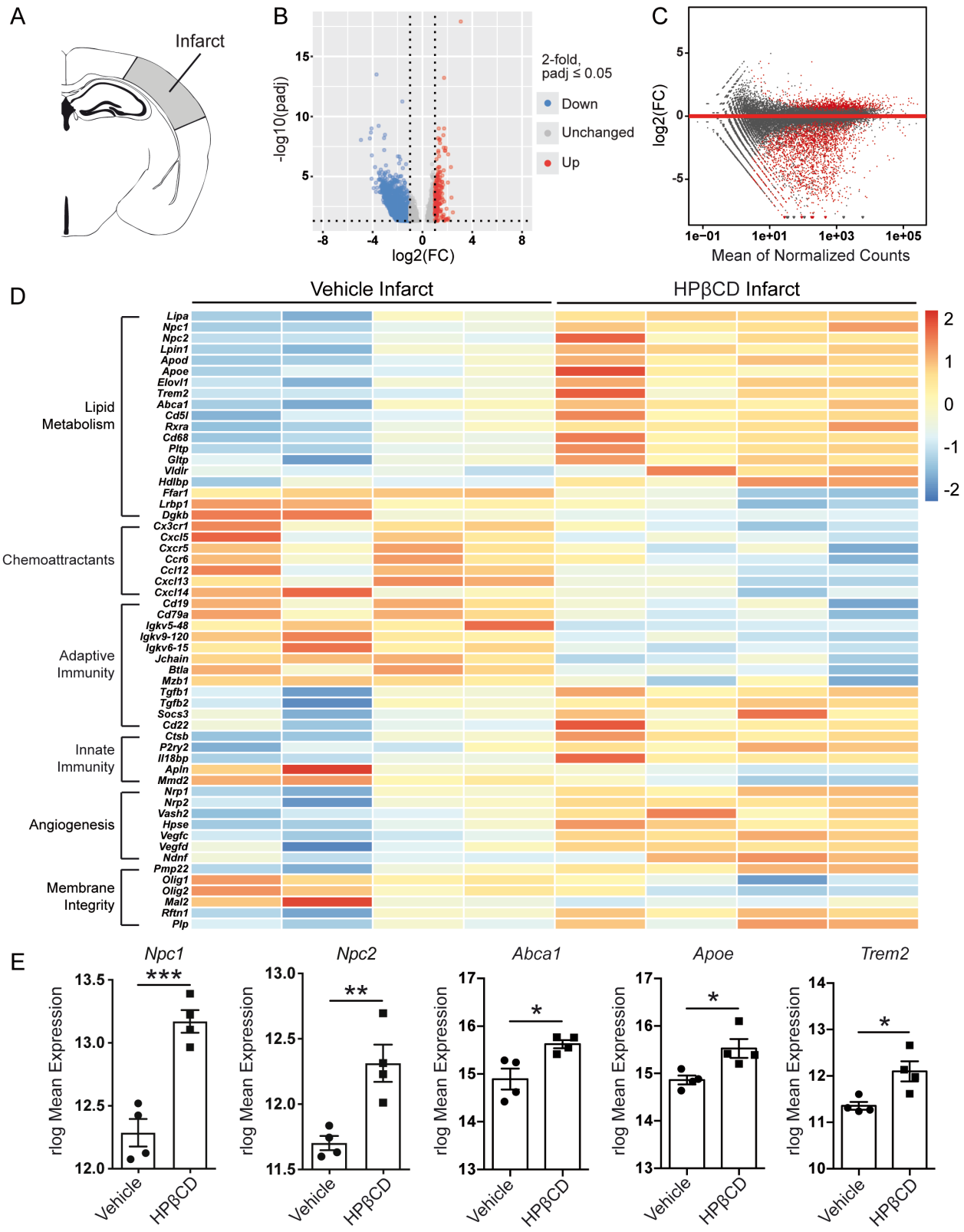

Figure 8. HPβCD promotes lipid metabolism and attenuates inflammation in infarcts of aged mice after stroke. ***A,*** Schematic of a mouse coronal brain section following stroke induced by distal middle cerebral artery occlusion + hypoxia, with the analyzed region shaded in gray. ***B, C,*** Volcano (***B***) and MA (***C***) plots constructed from count data show differences in gene expression between infarcts from vehicle- and HPβCD-treated mice at 7 weeks after stroke (false discovery rate-adjusted $p < 0.05$; FC > |2|). ***D,*** Row-scaled heatmap displaying differentially expressed genes associated with lipid metabolism, inflammation, and angiogenesis (false discovery rate-adjusted $p < 0.05$; FC > |2|). ***E,*** Graphs representing rlog-normalized expression of selected genes related to lipid metabolism. ($n = 4$; unpaired t tests; $^{*}p < 0.05$, $^{**}p < 0.01$, $^{***}p < 0.001$). FC, fold change.

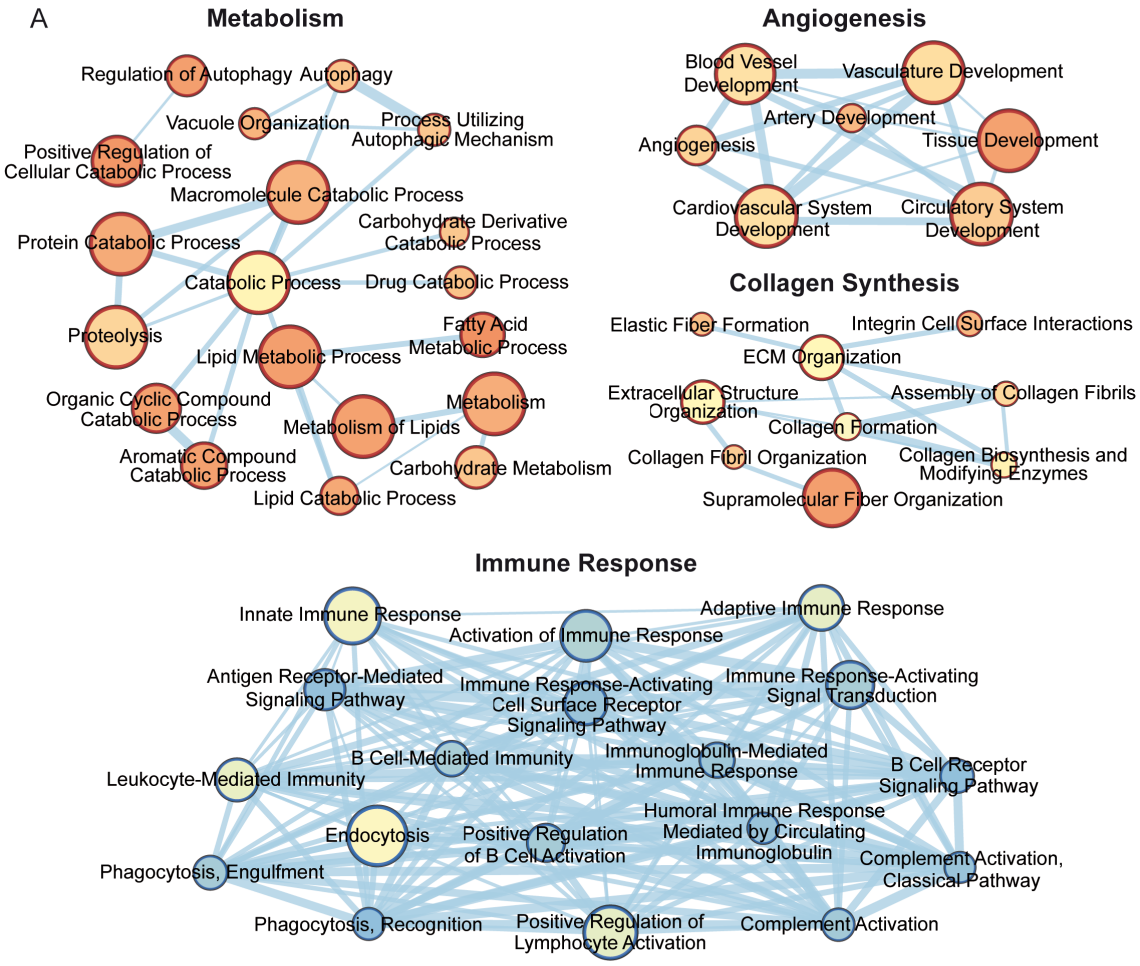

Figure 9. Biological processes enriched in infarcts of HPβCD-treated aged mice at 7 weeks after stroke. ***A,*** Enrichment maps constructed from Gene Ontology terms revealed a significant upregulation of metabolism, angiogenesis, and collagen synthesis pathways and a significant downregulation of immune response pathways. Pathways are shown as circles (nodes) that are connected with lines (edges) if the pathways share genes. Node colors are based on the enrichment score, and edge sizes are based on the number of genes shared by the connected pathways. ***B,*** Gene set enrichment analysis (GSEA) revealed significant enrichment of various biological processes in the infarcts of HPβCD-treated aged mice, depicted in red. Conversely, GSEA identified biological processes more significantly enriched in the infarcts of vehicle-injected mice compared to HPβCD-treated mice, depicted in blue.

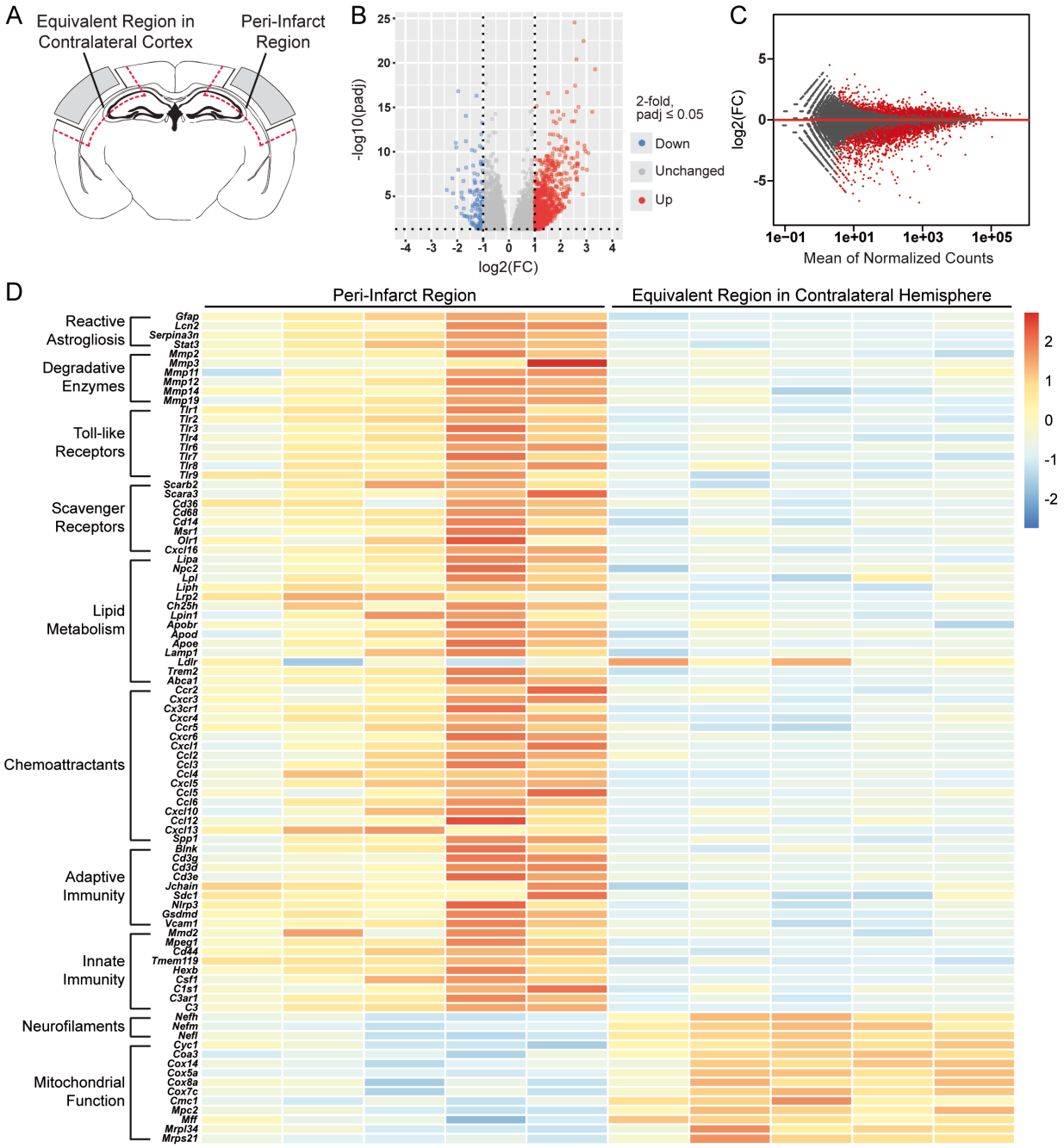

Figure 10. Transcriptome of the peri-infarct region in aged mice at 7 weeks after stroke. ***A,*** Schematic of a mouse coronal brain section following stroke induced by distal middle cerebral artery occlusion + hypoxia, with analyzed regions indicated. ***B, C,*** Volcano (***B***) and MA (***C***) plots constructed from count data show differences in gene

928 expression between peri-infarct regions and equivalent regions in the contralateral
929 cortex at 7 weeks after stroke (false discovery rate-adjusted $p < 0.05$; FC > |2|). ***D,*** Row-
930 scaled heatmap displaying differentially expressed genes associated with lipid
931 metabolism, inflammation, and mitochondrial function (false discovery rate-adjusted $p <$
932 0.05; FC > |2|). FC, fold change.

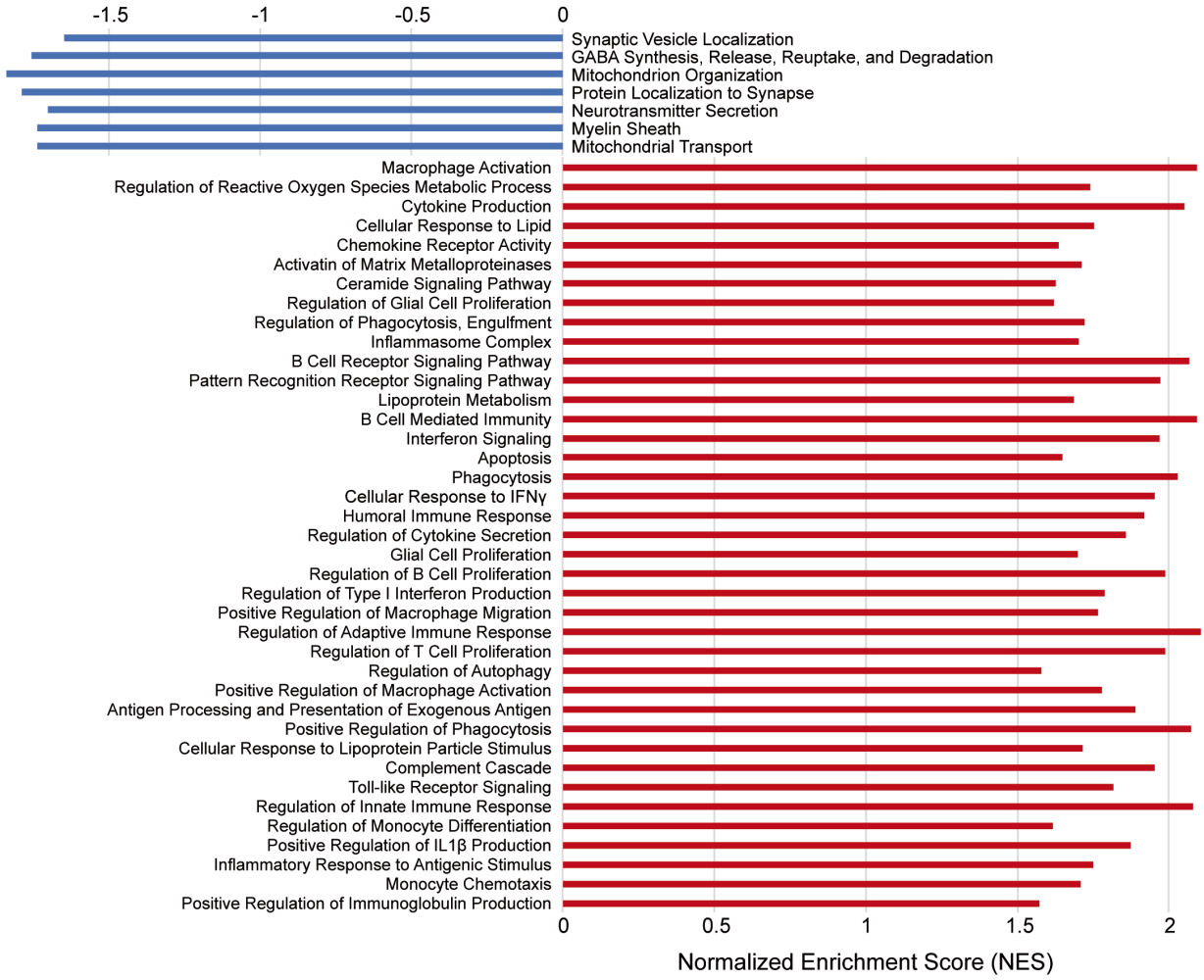

933

934 **Figure 11. Biological processes enriched in peri-infarct regions of aged mice at 7**

935 **weeks after stroke.** Gene set enrichment analysis (GSEA) revealed significant

936 enrichment of multiple biological processes in the peri-infarct regions of aged mice,

937 depicted in red. Conversely, GSEA identified biological processes more significantly

938 enriched in the equivalent region of the contralateral hemisphere, depicted in blue.

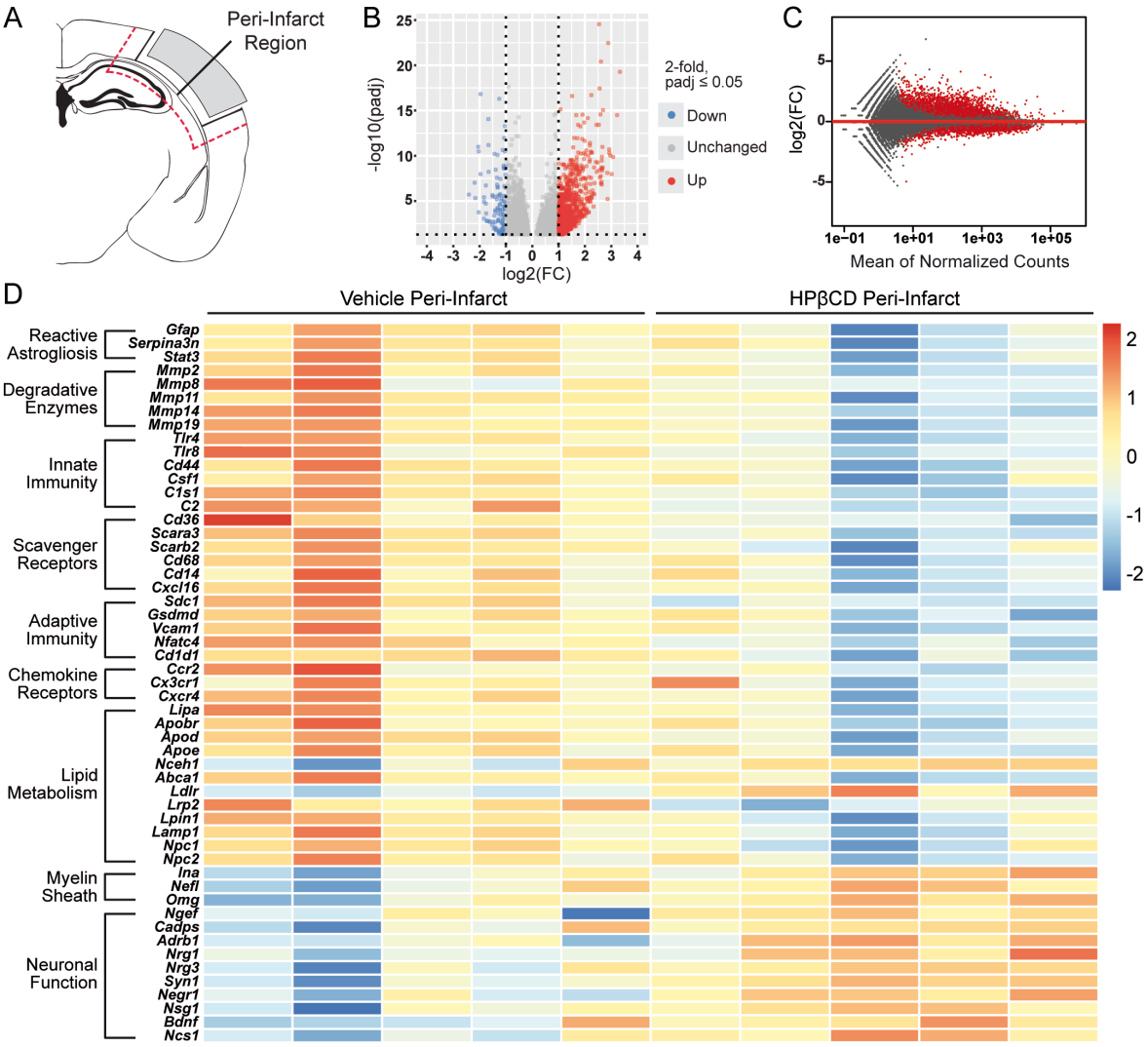

939

940 **Figure 12. HPβCD attenuates inflammation and increases transcripts associated**

941 **with neuronal function in peri-infarct regions of aged mice after stroke. *A,***

942 Schematic of a mouse coronal brain section following stroke induced by distal middle

943 cerebral artery occlusion + hypoxia, with the analyzed region indicated. ***B, C,*** Volcano

944 (***B***) and MA (***C***) plots constructed from count data show differences in gene expression

945 between peri-infarct regions from vehicle- and HPβCD-treated aged mice at 7 weeks

946 after stroke (false discovery rate-adjusted p < 0.05; FC > |2|). ***D,*** Row-scaled heatmap

947 displaying differentially expressed genes associated with lipid metabolism,

948 inflammation, and neuronal function (false discovery rate-adjusted $p < 0.05$; FC > |2|).

949 FC, fold change.

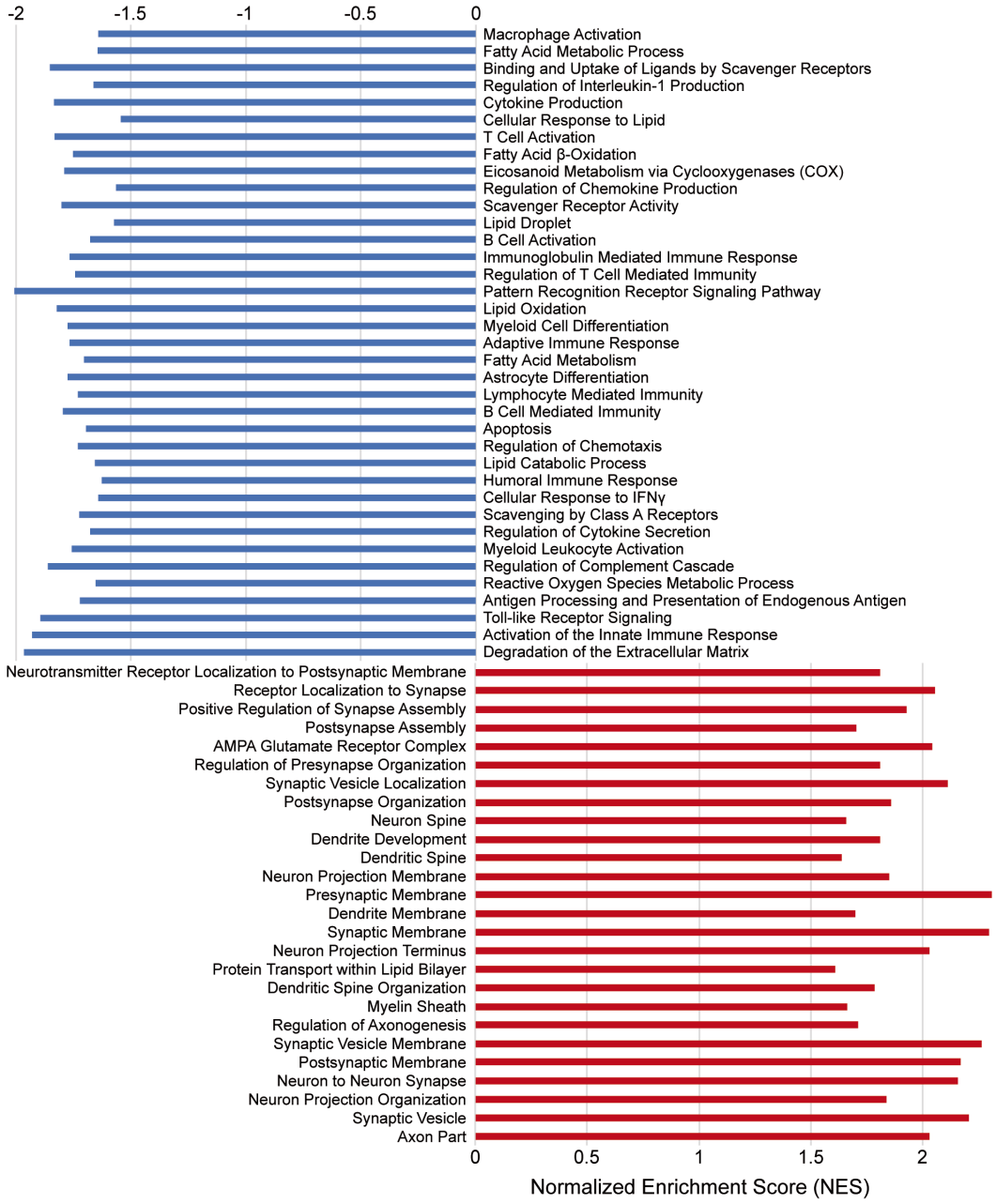

Figure 13. Biological processes enriched in peri-infarct regions of HPβCD-treated aged mice at 7 weeks after stroke. Gene set enrichment analysis (GSEA) revealed significant enrichment of multiple biological processes in peri-infarct regions of HPβCD-treated aged mice, depicted in red. Conversely, GSEA identified biological processes

more significantly enriched in peri-infarct regions of vehicle-injected aged mice, depicted in blue.

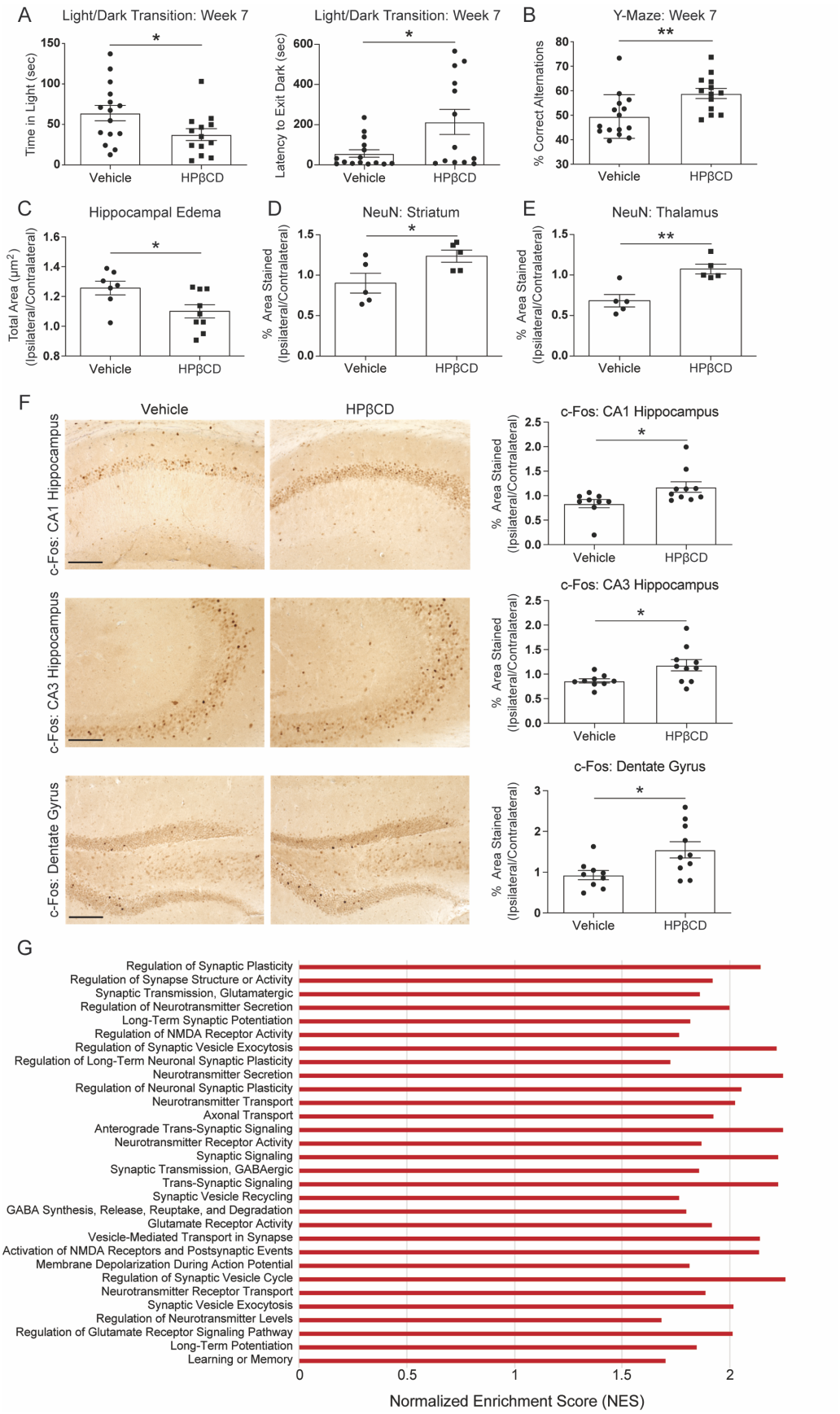

Figure 14. HPβCD attenuates neurodegeneration and improves recovery in aged mice after stroke. ***A,*** HPβCD-treated aged mice exhibited less impulsive behavior than vehicle-injected mice in the light/dark transition test at 7 weeks after stroke. (n = 13–15; unpaired t tests; *$p < 0.05$). ***B,*** HPβCD-treated aged mice exhibited intact spatial working memory in the Y-maze spontaneous alternation behavior test compared to vehicle-injected aged mice at 7 weeks after stroke. (n = 14–15; unpaired t test; *$p < 0.05$). ***C,*** Quantification of hippocampal edema at 7 weeks after stroke in vehicle- and HPβCD-treated mice. (n = 7–9; unpaired t test; *$p < 0.05$). ***D, E,*** Quantification of NeuN immunoreactivity in the striatum and thalamus from vehicle- or HPβCD-treated mice. (n = 5; unpaired t tests; *$p < 0.05$, **$p < 0.01$). ***F,*** Representative 20× images of c-Fos immunoreactivity in hippocampal regions from vehicle- or HPβCD-treated mice. Quantification of images is shown to the right of each photomicrograph. (n = 9–10; unpaired t tests; *$p < 0.05$, ***$p < 0.001$). Scale bar, 125 μm. Data are presented as mean ± SEM. ***G,*** Gene set enrichment analysis revealed significant enrichment of biological processes associated with neuronal function and activity in peri-infarct regions of HPβCD-treated aged mice at 7 weeks after stroke.

Figure	Group Size (*n*)	Statistical Test	Statistical Values	*p* value	*post hoc* Comparisons	*p* value
1A	4	Paired *t* test	*M* (Contra Cortex - Infarct) = -51.71 *SEM* = 1.300	< 0.0001	N/A	N/A
1B	Infarct = 7 Contra Cortex = 4	Unpaired *t* test	*M* (Contra Cortex - Infarct) = -34.14 *SEM* = 1.077	< 0.0001	N/A	N/A
1C	8	Multiple *t* tests; Holm-Sidak's multiple comparisons test	N/A	N/A	SM 14:0_16.51	0.000003
					SM 15:0_17.67	< 0.000001
					SM 16:0_19.05	< 0.000001
					SM 16:1_16.92	0.000003
					SM 16:1_17.23	0.000004
					SM 18:0_22.55	0.00379
					SM 18:1_19.71	0.000172
					SM 18:1_20.12	0.009913
					SM 19:0_24.48	0.002555
					SM 20:0_26.16	0.000813
					SM 20:1_23.41	0.0018
					SM 21:0_27.48	0.006607
					SM 22:0_28.28	< 0.000001
					SM 22:1_26.30	0.000006
					SM 22:1_26.87	0.000056
					SM 22:2_23.57	0.000003
					SM 23:0_28.82	0.002919
					SM 23:1_27.48	< 0.000001
					SM 23:2_25.37	0.000017
					SM 24:0_29.21	< 0.000001
					SM 24:1_28.23	< 0.000001
					SM 24:2_26.78	0.000062
					SM 24:3_24.26	0.000002
					SM 24:3_24.64	0.000004
					SM 24:4_22.21	0.000005
					SM 25:0_29.62	0.000226
					SM 26:0_29.96	0.000076
					SM 26:1_29.14	0.000001
					SM 26:2_28.42	0.00016
2A	4	Paired *t* test	*M* (Contra Cortex - Infarct) = -54.83 *SEM* = 1.527	< 0.0001	N/A	N/A
2B	9	Paired *t* test	*M* (Contra Cortex - Infarct) = -27.39	< 0.0001	N/A	N/A

			SEM = 0.9784			
2C	5	Multiple *t* tests; Holm-Sidak's multiple comparisons test	N/A	N/A	CE 12:0	0.007817
					CE 14:0	0.000752
					CE 15:0	0.003201
					CE 16:0	0.000217
					CE 16:1	0.000495
					CE 17:0	0.001331
					CE 18:0	0.000894
					CE 18:1	0.001131
					CE 18:2	0.001921
					CE 18:3	0.001145
					CE 20:0	0.005071
					CE 20:3	0.001136
					CE 20:4	0.000936
					CE 20:5	0.000785
					CE 22:0	0.00243
					CE 22:6	0.005786
					CE 24:0	0.007793
					CE 24:1	0.000802
5B (B220)	Vehicle = 11	Unpaired *t* test	*M* (HPβCD - Vehicle) = -12.22	< 0.0001	N/A	N/A
	HPβCD = 10		*SEM* = 1.819			
5B (CD3ε)	Vehicle = 11	Unpaired *t* test	*M* (HPβCD - Vehicle) = -7.695	< 0.0001	N/A	N/A
	HPβCD = 10		*SEM* = 0.9035			
5B (CD138)	4	Unpaired *t* test	*M* (HPβCD - Vehicle) = -51.22	0.0163	N/A	N/A
			SEM = 15.49			
5B (IgA)	8	Unpaired *t* test	*M* (HPβCD - Vehicle) = -34.30	0.0026	N/A	N/A
			SEM = 9.362			
5B (ORO)	4	Unpaired *t* test	*M* (HPβCD - Vehicle) = -4.999	0.0462	N/A	N/A
			SEM = 1.995			
6B (B220)	Vehicle = 4	Unpaired *t* test	*M* (HPβCD - Vehicle) = -6.580	0.0039	N/A	N/A
	HPβCD = 5		*SEM* = 0.8794			
6B (CD3ε)	Vehicle = 8	Unpaired *t* test	*M* (HPβCD - Vehicle) = -12.75	0.0002	N/A	N/A
	HPβCD = 7		*SEM* = 2.429			
6B (IgA)	Vehicle = 5	Unpaired *t* test	*M* (HPβCD - Vehicle) = -21.55	0.0477	N/A	N/A
	HPβCD = 6		*SEM* = 8.139			
6B (ORO)	4	Unpaired *t* test	*M* (HPβCD - Vehicle) = -9.330	0.0002	N/A	N/A

			SEM = 1.124			
6B (Alcian Blue)	Vehicle = 9 HPβCD = 10	Unpaired *t* test	*M* (HPβCD - Vehicle) = -1.372 *SEM* = 1.954	0.4921	N/A	N/A
7B (CD19+GL7-)	Vehicle = 10 HPβCD = 9	Unpaired *t* test	*M* (HPβCD - Vehicle) = 3.258 *SEM* = 2.553	0.2191	N/A	N/A
7B (CD19+GL7+)	Vehicle = 10 HPβCD = 9	Unpaired *t* test	*M* (HPβCD - Vehicle) = -0.1013 *SEM* = 0.1402	0.4796	N/A	N/A
7C (IgG1)	Vehicle = 10 HPβCD = 9	Unpaired *t* test	*M* (HPβCD - Vehicle) = -2.589 *SEM* = 28.71	0.9292	N/A	N/A
7C (IgA)	Vehicle = 10 HPβCD = 9	Unpaired *t* test	*M* (HPβCD - Vehicle) = 7.567 *SEM* = 16.23	0.647	N/A	N/A
7E (CD4+ T cells)	9	Unpaired *t* test	*M* (HPβCD - Vehicle) = 0.03444 *SEM* = 0.9497	0.9715	N/A	N/A
7E (CD8+ T cells)	9	Unpaired *t* test	*M* (HPβCD - Vehicle) = -0.08889 *SEM* = 1.201	0.9419	N/A	N/A
7E (Tregs)	9	Unpaired *t* test	*M* (HPβCD - Vehicle) = -1.844 *SEM* = 2.238	0.422	N/A	N/A
7F	6	Multiple *t* tests; Holm-Sidak's multiple comparisons test	N/A	N/A	WBC Neutrophils Lymphocytes Monocytes Eosinophils Basophils	0.109564 0.213092 0.0445 0.027171 0.662546 0.58393
8E (*Npc1*)	4	Unpaired *t* test	*M* (HPβCD - Vehicle) = 0.8853 *SEM* = 0.1417	0.0008	N/A	N/A
8E (*Npc2*)	4	Unpaired *t* test	*M* (HPβCD - Vehicle) = 0.6104 *SEM* = 0.1525	0.0071	N/A	N/A
8E (*Abca1*)	4	Unpaired *t* test	*M* (HPβCD - Vehicle) = 0.7311 *SEM* = 0.2348	0.0208	N/A	N/A
8E (*Apoe*)	4	Unpaired *t* test	*M* (HPβCD - Vehicle) = 0.6647 *SEM* = 0.2186	0.0228	N/A	N/A
8E (*Trem2*)	4	Unpaired *t* test	*M* (HPβCD - Vehicle) = 0.7428 *SEM* = 0.2325	0.0187	N/A	N/A
14A (Time)	Vehicle = 15	Unpaired *t* test	*M* (HPβCD - Vehicle) = -26.63	0.0393	N/A	N/A

	HPβCD = 13		*SEM* = 12.27			
14A (Latency)	Vehicle = 15	Unpaired *t* test	*M* (HPβCD - Vehicle) = 157.5	0.0165	N/A	N/A
	HPβCD = 13		*SEM* = 61.44			
14B	Vehicle = 15	Unpaired *t* test	*M* (HPβCD - Vehicle) = 8.520	0.0113	N/A	N/A
	HPβCD = 14		*SEM* = 3.133			
14C	Vehicle = 7	Unpaired *t* test	*M* (HPβCD - Vehicle) = -0.1564	0.0311	N/A	N/A
	HPβCD = 9		*SEM* = 0.06527			
14D	5	Unpaired *t* test	*M* (HPβCD - Vehicle) = 0.3339	0.0487	N/A	N/A
			SEM = 0.1438			
14E	5	Unpaired *t* test	*M* (HPβCD - Vehicle) = 0.3901	0.0039	N/A	N/A
			SEM = 0.09717			
14F (CA1 Hippocampus)	Vehicle = 9	Unpaired *t* test	*M* (HPβCD - Vehicle) = 0.3379	0.0268	N/A	N/A
	HPβCD = 10		*SEM* = 0.1394			
14F (CA3 Hippocampus)	Vehicle = 9	Unpaired *t* test	*M* (HPβCD - Vehicle) = 0.3196	0.0229	N/A	N/A
	HPβCD = 10		*SEM* = 0.1278			
14F (Dentate Gyrus)	Vehicle = 9	Unpaired *t* test	*M* (HPβCD - Vehicle) = 0.6193	0.0178	N/A	N/A
	HPβCD = 10		*SEM* = 0.2362			

974 **Table 1. Statistical table.**

975 **References**

976 Albertini, G., Walrave, L., Demuyser, T., Massie, A., De Bundel, D., & Smolders, I.
977 (2018). 6 Hz corneal kindling in mice triggers neurobehavioral comorbidities
978 accompanied by relevant changes in c-Fos immunoreactivity throughout the brain.
979 *Epilepsia*, *59*(1), 67–78. https://doi.org/10.1111/epi.13943
980 Anders, S., Pyl, P. T., & Huber, W. (2015). HTSeq-A Python framework to work with
981 high-throughput sequencing data. *Bioinformatics*.
982 https://doi.org/10.1093/bioinformatics/btu638
983 Ankeny, D. P., Lucin, K. M., Sanders, V. M., McGaughy, V. M., & Popovich, P. G.
984 (2006). Spinal cord injury triggers systemic autoimmunity: evidence for chronic B
985 lymphocyte activation and lupus-like autoantibody synthesis. *Journal of*
986 *Neurochemistry*, *99*(4), 1073–1087. https://doi.org/10.1111/j.1471-
987 4159.2006.04147.x
988 Aslanian, A. M., & Charo, I. F. (2006). Targeted disruption of the scavenger receptor
989 and chemokine CXCL16 accelerates atherosclerosis. *Circulation*.
990 https://doi.org/10.1161/CIRCULATIONAHA.105.540583
991 Black, S. E. (2011). Vascular cognitive impairment: Epidemiology, subtypes, diagnosis
992 and management. *Journal of the Royal College of Physicians of Edinburgh*, *41*(1),
993 49–56. https://doi.org/10.4997/JRCPE.2011.121
994 Bolger, A. M., Lohse, M., & Usadel, B. (2014). Trimmomatic: A flexible trimmer for
995 Illumina sequence data. *Bioinformatics*.
996 https://doi.org/10.1093/bioinformatics/btu170
997 Bourin, M., & Hascoët, M. (2003, February 28). The mouse light/dark box test.

European Journal of Pharmacology. Elsevier. https://doi.org/10.1016/S0014-2999(03)01274-3

Cantuti-Castelvetri, L., Fitzner, D., Bosch-Queralt, M., Weil, M. T., Su, M., Sen, P., … Simons, M. (2018). Defective cholesterol clearance limits remyelination in the aged central nervous system. *Science*. https://doi.org/10.1126/science.aan4183

Chung, A. G., Frye, J. B., Zbesko, J. C., Constantopoulos, E., Hayes, M., Figueroa, A. G., … Doyle, K. P. (2018). Liquefaction of the brain following stroke shares a similar molecular and morphological profile with atherosclerosis and mediates secondary neurodegeneration in an osteopontin-dependent mechanism. *ENeuro*, *5*(5). https://doi.org/10.1523/ENEURO.0076-18.2018

Dietschy, J. M., & Turley, S. D. (2001). Cholesterol metabolism in the brain. *Current Opinion in Lipidology*. https://doi.org/10.1097/00041433-200104000-00003

Dobin, A., Davis, C. A., Schlesinger, F., Drenkow, J., Zaleski, C., Jha, S., … Gingeras, T. R. (2013). STAR: Ultrafast universal RNA-seq aligner. *Bioinformatics*. https://doi.org/10.1093/bioinformatics/bts635

Doyle, K. P., Quach, L. N., Sole, M., Axtell, R. C., Nguyen, T.-V. V., Soler-Llavina, G. J., … Buckwalter, M. S. (2015). B-Lymphocyte-Mediated Delayed Cognitive Impairment following Stroke. *Journal of Neuroscience*, *35*(5), 2133–2145. https://doi.org/10.1523/JNEUROSCI.4098-14.2015

Doyle, Kristian P., Fathali, N., Siddiqui, M. R., & Buckwalter, M. S. (2012). Distal hypoxic stroke: A new mouse model of stroke with high throughput, low variability and a quantifiable functional deficit. *Journal of Neuroscience Methods*. https://doi.org/10.1016/j.jneumeth.2012.03.003

1021 Febbraio, M., Hajjar, D. P., & Silverstein, R. L. (2001). CD36: A class B scavenger
1022 receptor involved in angiogenesis, atherosclerosis, inflammation, and lipid
1023 metabolism. *Journal of Clinical Investigation*. https://doi.org/10.1172/JCI14006
1024 Fitzner, D., Bader, J. M., Penkert, H., Bergner, C. G., Su, M., Weil, M. T., … Simons, M.
1025 (2020). Cell-Type- and Brain-Region-Resolved Mouse Brain Lipidome. *Cell*
1026 *Reports*. https://doi.org/10.1016/j.celrep.2020.108132
1027 Fleischmann, A., Hvalby, O., Jensen, V., Strekalova, T., Zacher, C., Layer, L. E., …
1028 Gass, P. (2003). Impaired long-term memory and NR2A-type NMDA receptor-
1029 dependent synaptic plasticity in mice lacking c-fos in the CNS. *Journal of*
1030 *Neuroscience*, *23*(27), 9116–9122. https://doi.org/10.1523/jneurosci.23-27-
1031 09116.2003
1032 Gaspar, J., Mathieu, J., & Alvarez, P. (2017). 2-Hydroxypropyl-beta-cyclodextrin
1033 (HPβCD) reduces age-related lipofuscin accumulation through a cholesterol-
1034 associated pathway. *Scientific Reports*. https://doi.org/10.1038/s41598-017-02387-
1035 8
1036 Ghosh, S., Zhao, B., Bie, J., & Song, J. (2010). Macrophage cholesteryl ester
1037 mobilization and atherosclerosis. *Vascular Pharmacology*.
1038 https://doi.org/10.1016/j.vph.2009.10.002
1039 Gidwani, B., & Vyas, A. (2015). A Comprehensive Review on Cyclodextrin-Based
1040 Carriers for Delivery of Chemotherapeutic Cytotoxic Anticancer Drugs. *BioMed*
1041 *Research International*. https://doi.org/10.1155/2015/198268
1042 Go, G. W., & Mani, A. (2012). Low-density lipoprotein receptor (LDLR) family
1043 orchestrates cholesterol homeostasis. *Yale Journal of Biology and Medicine*.

1044 Goldberg, I. J., Reue, K., Abumrad, N. A., Bickel, P. E., Cohen, S., Fisher, E. A., …
1045 Chen, J. (2018). Deciphering the role of lipid droplets in cardiovascular disease.
1046 *Circulation*. https://doi.org/10.1161/CIRCULATIONAHA.118.033704
1047 Liscic, R. M., Storandt, M., Cairns, N. J., & Morris, J. C. (2007). Clinical and
1048 psychometric distinction of frontotemporal and Alzheimer dementias. *Archives of*
1049 *Neurology*, *64*(4), 535–540. https://doi.org/10.1001/archneur.64.4.535
1050 Love, M. I., Huber, W., & Anders, S. (2014). Moderated estimation of fold change and
1051 dispersion for RNA-seq data with DESeq2. *Genome Biology*.
1052 https://doi.org/10.1186/s13059-014-0550-8
1053 Luchtman, D. W., & Song, C. (2013). Cognitive enhancement by omega-3 fatty acids
1054 from child-hood to old age: Findings from animal and clinical studies.
1055 *Neuropharmacology*. https://doi.org/10.1016/j.neuropharm.2012.07.019
1056 Mar, F. M., da Silva, T. F., Morgado, M. M., Rodrigues, L. G., Rodrigues, D., Pereira, M.
1057 I. L., … Brites, P. (2016). Myelin Lipids Inhibit Axon Regeneration Following Spinal
1058 Cord Injury: a Novel Perspective for Therapy. *Molecular Neurobiology*.
1059 https://doi.org/10.1007/s12035-014-9072-3
1060 Matsuo, M., Togawa, M., Hirabaru, K., Mochinaga, S., Narita, A., Adachi, M., … Ohno,
1061 K. (2013). Effects of cyclodextrin in two patients with Niemann-Pick Type C
1062 disease. *Molecular Genetics and Metabolism*.
1063 https://doi.org/10.1016/j.ymgme.2012.11.005
1064 Merico, D., Isserlin, R., Stueker, O., Emili, A., & Bader, G. D. (2010). Enrichment map: A
1065 network-based method for gene-set enrichment visualization and interpretation.
1066 *PLoS ONE*. https://doi.org/10.1371/journal.pone.0013984

1067 Nguyen, T. V. V., Frye, J. B., Zbesko, J. C., Stepanovic, K., Hayes, M., Urzua, A., …
1068 Doyle, K. P. (2016). Multiplex immunoassay characterization and species
1069 comparison of inflammation in acute and non-acute ischemic infarcts in human and
1070 mouse brain tissue. *Acta Neuropathologica Communications*, *4*(1), 100.
1071 https://doi.org/10.1186/s40478-016-0371-y
1072 Nguyen, T. V. V., Hayes, M., Zbesko, J. C., Frye, J. B., Congrove, N. R., Belichenko, N.
1073 P., … Doyle, K. P. (2018). Alzheimer's associated amyloid and tau deposition co-
1074 localizes with a homeostatic myelin repair pathway in two mouse models of post-
1075 stroke mixed dementia. *Acta Neuropathologica Communications*, *6*(1), 100.
1076 https://doi.org/10.1186/s40478-018-0603-4
1077 Ortega, S. B., Noorbhai, I., Poinsatte, K., Kong, X., Anderson, A., Monson, N. L., &
1078 Stowe, A. M. (2015). Stroke induces a rapid adaptive autoimmune response to
1079 novel neuronal antigens. *Discov Med*, *19*(106), 381–392.
1080 Park, Y. M. (2014). CD36, a scavenger receptor implicated in atherosclerosis.
1081 *Experimental and Molecular Medicine*. https://doi.org/10.1038/emm.2014.38
1082 Poitelon, Y., Kopec, A. M., & Belin, S. (2020). Myelin Fat Facts: An Overview of Lipids
1083 and Fatty Acid Metabolism. *Cells*. https://doi.org/10.3390/cells9040812
1084 Quehenberger, O., Armando, A. M., Brown, A. H., Milne, S. B., Myers, D. S., Merrill, A.
1085 H., … Dennis, E. A. (2010). Lipidomics reveals a remarkable diversity of lipids in
1086 human plasma. *Journal of Lipid Research*. https://doi.org/10.1194/jlr.M009449
1087 Rahaman, S. O., Lennon, D. J., Febbraio, M., Podrez, E. A., Hazen, S. L., & Silverstein,
1088 R. L. L. (2006). A CD36-dependent signaling cascade is necessary for macrophage
1089 foam cell formation. *Cell Metabolism*. https://doi.org/10.1016/j.cmet.2006.06.007

1090 Raine, C. S., Cannella, B., Hauser, S. L., & Genain, C. P. (1999). Demyelination in
1091 primate autoimmune encephalomyelitis and acute multiple sclerosis lesions: A case
1092 for antigen-specific antibody mediation. *Annals of Neurology*, *46*(2), 144–160.
1093 https://doi.org/10.1002/1531-8249(199908)46:2<144::AID-ANA3>3.0.CO;2-K
1094 Rasheed, A., Kumar C.K., A., & Sravanthi, V. V. N. S. S. (2008). Cyclodextrins as drug
1095 carrier molecule: A review. *Scientia Pharmaceutica*.
1096 https://doi.org/10.3797/scipharm.0808-05
1097 Schindelin, J., Arganda-Carreras, I., Frise, E., Kaynig, V., Longair, M., Pietzsch, T., …
1098 Cardona, A. (2012, July). Fiji: An open-source platform for biological-image
1099 analysis. *Nature Methods*. NIH Public Access. https://doi.org/10.1038/nmeth.2019
1100 Seifert, H. A., Hall, A. A., Chapman, C. B., Collier, L. A., Willing, A. E., & Pennypacker,
1101 K. R. (2012). A Transient Decrease in Spleen Size Following Stroke Corresponds
1102 to Splenocyte Release into Systemic Circulation. *Journal of Neuroimmune*
1103 *Pharmacology 2012 7:4*, *7*(4), 1017–1024. https://doi.org/10.1007/S11481-012-
1104 9406-8
1105 Takao, K., & Miyakawa, T. (2006). Light/dark transition test for mice. *Journal of*
1106 *Visualized Experiments*, (1), 104. https://doi.org/10.3791/104
1107 Taylor, A. M., Liu, B., Mari, Y., Liu, B., & Repa, J. J. (2012). Cyclodextrin mediates rapid
1108 changes in lipid balance in Npc1-/- mice without carrying cholesterol through the
1109 bloodstream. *Journal of Lipid Research*. https://doi.org/10.1194/jlr.M028241
1110 Vance, J. E. (2012). Dysregulation of cholesterol balance in the brain: Contribution to
1111 neurodegenerative diseases. *DMM Disease Models and Mechanisms*.
1112 https://doi.org/10.1242/dmm.010124

Virani, S. S., Alonso, A., Benjamin, E. J., Bittencourt, M. S., Callaway, C. W., Carson, A. P., … Heard, D. G. (2020). Heart disease and stroke statistics—2020 update: A report from the American Heart Association. *Circulation*. https://doi.org/10.1161/CIR.0000000000000757

Winzeler, A. M., Mandemakers, W. J., Sun, M. Z., Stafford, M., Phillips, C. T., & Barres, B. A. (2011). The lipid sulfatide is a novel myelin-associated inhibitor of CNS axon outgrowth. *Journal of Neuroscience*. https://doi.org/10.1523/JNEUROSCI.3004-10.2011

Yamada, K., Noda, Y., Hasegawa, T., Komori, Y., Nikai, T., Sugihara, H., & Nabeshima, T. (1996). The role of nitric oxide in dizocilpine-induced impairment of spontaneous alternation behavior in mice. *Journal of Pharmacology and Experimental Therapeutics*.

Yang, Y., Hu, F., Yang, G., & Meng, Q. (2020). Lack of sphingomyelin synthase 2 reduces cerebral ischemia/reperfusion injury by inhibiting microglial inflammation in mice. *Experimental and Therapeutic Medicine*, *20*(6). https://doi.org/10.3892/etm.2020.9371

Yu, X. H., Fu, Y. C., Zhang, D. W., Yin, K., & Tang, C. K. (2013). Foam cells in atherosclerosis. *Clinica Chimica Acta; International Journal of Clinical Chemistry*. https://doi.org/10.1016/j.cca.2013.06.006 [doi]

Zamanian, J. L., Xu, L., Foo, L. C., Nouri, N., Zhou, L., Giffard, R. G., & Barres, B. A. (2012). Genomic analysis of reactive astrogliosis. *Journal of Neuroscience*. https://doi.org/10.1523/JNEUROSCI.6221-11.2012

Zbesko, J.C., Frye, J. B., Becktel, D. A., Gerardo, D. K., Stokes, J., Calderon, K., …

1136 Doyle, K. P. (2020). IgA natural antibodies are produced following T-cell
1137 independent B-cell activation following stroke. *Brain, Behavior, and Immunity*.
1138 https://doi.org/10.1016/j.bbi.2020.09.014
1139 Zbesko, Jacob C., Nguyen, T. V. V., Yang, T., Frye, J. B., Hussain, O., Hayes, M., …
1140 Doyle, K. P. (2018). Glial scars are permeable to the neurotoxic environment of
1141 chronic stroke infarcts. *Neurobiology of Disease*.
1142 https://doi.org/10.1016/j.nbd.2018.01.007
1143 Zeibig, S., Büttcher, M., Goebel, S., Pauli, J., Hunger, A., Ungerer, M., … Münch, G.
1144 (2019). The scavenger receptor CD68 regulates platelet mediated oxidized low-
1145 density lipoprotein (oxLDL) deposition in atherosclerotic vessels at an early stage of
1146 atherosclerosis in LDLr-/-/ApoBec-/- mice. *Cellular Physiology and Biochemistry*.
1147 https://doi.org/10.33594/000000048
1148 Zhu, Y., Lyapichev, K., Lee, D. H., Motti, D., Ferraro, N. M., Zhang, Y., … Lee, J. K.
1149 (2017). Macrophage Transcriptional Profile Identifies Lipid Catabolic Pathways That
1150 Can Be Therapeutically Targeted after Spinal Cord Injury. *The Journal of*
1151 *Neuroscience*. https://doi.org/10.1523/JNEUROSCI.2751-16.2017
1152 Zimmer, S., Grebe, A., Bakke, S. S., Bode, N., Halvorsen, B., Ulas, T., … Latz, E.
1153 (2016). Cyclodextrin promotes atherosclerosis regression via macrophage
1154 reprogramming. *Science Translational Medicine*, *8*(333).
1155 https://doi.org/10.1126/scitranslmed.aad6100
1156